

A thermodynamically consistent phase-field model for two-phase flows with thermocapillary effects

Z. Guo^{1,2} and P. Lin^{1,†}

¹Department of Mathematics, University of Dundee, Dundee DD1 4HN, Scotland, UK

²Department of Applied Mathematics and Mechanics, University of Science and Technology Beijing, Beijing 100083, China

(Received 18 February 2014; revised 10 October 2014; accepted 27 November 2014;
first published online 4 February 2015)

In this paper, we develop a phase-field model for binary incompressible (quasi-incompressible) fluid with thermocapillary effects, which allows for the different properties (densities, viscosities and heat conductivities) of each component while maintaining thermodynamic consistency. The governing equations of the model including the Navier–Stokes equations with additional stress term, Cahn–Hilliard equations and energy balance equation are derived within a thermodynamic framework based on entropy generation, which guarantees thermodynamic consistency. A sharp-interface limit analysis is carried out to show that the interfacial conditions of the classical sharp-interface models can be recovered from our phase-field model. Moreover, some numerical examples including thermocapillary convections in a two-layer fluid system and thermocapillary migration of a drop are computed using a continuous finite element method. The results are compared with the corresponding analytical solutions and the existing numerical results as validations for our model.

Key words: drops, multiphase flow, thermocapillarity

1. Introduction

When the interface separating two fluids is exposed to a temperature gradient, the variations of surface tension along the interface lead to shear stresses that act on the fluid through viscous forces, and thus induce a motion of the fluids in the direction of the temperature gradient. For most fluids, the surface tension generally decreases with increasing temperature. The non-uniformity of surface tension then drives the fluids to move from the region with higher temperature to that with lower temperature. This effect is known as the thermocapillary (Marangoni) effect (Levich 1962), and it plays an important role in various industrial applications involving microgravity (Subramanian & Balasubramaniam 2001) or microdevices (Darhuber & Troian 2005), where the surface forces become dominant. One famous example of thermocapillary effects is the thermocapillary migration of drops, where the drops

† Email address for correspondence: plin@maths.dundee.ac.uk

are set in a liquid possessing a temperature gradient, and will move towards the hot region due to the thermocapillary effects. The thermocapillary migration of a drop was first examined experimentally by Young, Goldstein & Block (1959), who derived an analytical expression for the terminal velocity of a single spherical drop in a constant temperature gradient by assuming that the convective transport of momentum and energy are negligible. Since then, extensive works have been carried out experimentally, analytically and numerically in order to investigate this phenomenon; many of them are summarized by Subramanian & Balasubramaniam (2001). Another example of thermocapillary effects is the thermocapillary convection in a two-layer fluid system (thermocapillary instabilities), where the system is typically confined between two parallel plates and subjected to a temperature gradient. Due to the perturbations in the temperature and velocity field as well as the interface position, surface tension gradients will occur at the interface and drive the fluid to motion. Instabilities then set in and lead to convective motion, where a typical convection pattern is the hexagonal cell formation found by Bénard (1900). Thermocapillary instabilities are widely studied, which can be traced back to some pioneering works performed by Block (1956), Pearson (1958), Sternling & Scriven (1959) and Scriven & Sternling (1964). Literature reviews of recent experimental and analytical work on instabilities in thermocapillary convection are provided by Davis (1987), Andereck *et al.* (1998) and Schatz & Neitzel (2001).

The problem described above is the multiphase flow problem, and the available numerical methods can roughly be divided into two categories: interface tracking and interface capturing methods. In interface tracking methods, the position of the interface is explicitly tracked, which requires meshes that track the interfaces and are updated as the flow evolves. Boundary-integral methods (see the review by Hou, Lowengrub & Shelley 2001), front-tracking methods (see the reviews by Tryggvason *et al.* 2001 and Hua, Stene & Lin 2008) and immersed-boundary methods (see the review by Mittal & Iaccarino 2005) are examples of this type. In the context of thermocapillary (Marangoni) effects, e.g. thermocapillary migration and thermocapillary instabilities, several works have been performed by using interface tracking methods. Here, we refer to the work of Zhou & Davis (1996), Berejnov, Lavrenteva & Nir (2001) and Rother, Zinchenko & Davis (2002) as examples for boundary-integral methods, Tavener & Cliffe (2002), Nas & Tryggvason (2003), Nas, Muradoglu & Tryggvason (2006) and Yin *et al.* (2008) for front-tracking methods and Blyth & Pozrikidis (2004) and Pozrikidis (2004) for immersed-boundary methods. In interface capturing methods, on the other hand, the interface is not tracked explicitly, but instead is implicitly defined through an interface function (e.g. level-set, colour or phase-field function). This means that the computations are based on fixed spatial domains and thus eliminate the problem of updating the meshes encountered in interface tracking methods. For example, volume-of-fluid (VOF) methods (see Scardovelli & Zaleski (1999) for a review, and Gambaryan-Roisman, Alexeev & Stephan 2005 and Ma & Bothe 2013 as examples for thermocapillary effects) and level-set methods (see Osher & Fedkiw 2001 and Sethian & Smereka 2003 for reviews, and Haj-Hariri, Shi & Borhan 1997 and Herrmann *et al.* 2008 as examples for thermocapillary effects) are of this type.

Another interface capturing method is the phase-field method, or diffuse-interface method (see, for reviews, Anderson, McFadden & Wheeler 1998, Emmerich 2008 and Kim 2012), which has now emerged as a powerful method to simulate many types of multiphase flows, including drop coalescence, breakup, rising and deformations in shear flows (Jacqmin 1999; Boyer 2002; Lee, Lowengrub & Goodman 2002a,b;

Liu & Shen 2002; Baldalassi, Cenicerros & Banerjee 2004; Yue *et al.* 2004; Kim & Lowengrub 2005; Yue *et al.* 2006; Ding, Spelt & Shu 2007; Shen & Yang 2009; Hua *et al.* 2011; Guo, Lin & Lowengrub 2014a), phase separation (Baldalassi *et al.* 2004; Kim, Kang & Lowengrub 2004; Kim 2005), contact line dynamics (Jacqmin 2000; Qian, Wang & Sheng 2006; He, Glowinski & Ping 2011; Bao *et al.* 2012; Gao & Wang 2012; Yue & Feng 2012; Jiang & Lin 2014), dynamics of interfaces with surfactant adsorption (van der Sman & van der Graaf 2006; Teigen *et al.* 2011) and thermocapillary effects (Jasnaw & Vinals 1996; Borcia & Bestehorn 2003; Borcia, Merkt & Bestehorn 2004; Sun, Liu & Xu 2009; Guo, Lin & Wang 2014b). Phase-field methods are based on models of fluid free energy, which goes back to the work of Gibbs (1875), Cahn & Hilliard (1958), Cahn & Allen (1978) and van der Waals (1979). The basic idea of the phase-field method is to treat the multiphase fluid as one fluid with variable material properties. An order parameter is employed to characterize the different phases, which varies continuously over thin interfacial layers and is mostly uniform in the bulk phases. Sharp interfaces are then replaced by thin but non-zero-thickness transition regions, where the interfacial forces are smoothly distributed. One set of governing equations for the mixture can be derived variationally from its energy density field, where the order parameter fields satisfy an advection–diffusion equation (usually the advective Cahn–Hilliard equations) and are coupled to the Navier–Stokes equations through extra reactive stresses that mimic surface tension.

The classical phase-field model, in the case of two incompressible viscous Newtonian fluids, is the so-called model H (Hohenberg & Halperin 1977), which couples fluid flow with Cahn–Hilliard diffusion with a conserved parameter. It has been successfully used to simulate complicated mixing flows involving binary incompressible fluid with the same densities for both components (see, for example, Chella & Vinals 1996). Gurtin, Poligone & Vinale (1996) rederived this model in the framework of classical continuum mechanics and showed that it is consistent with the second law of thermodynamics in a mechanical version based on a local dissipation inequality.

One of the fundamental assumptions when deriving model H is that the binary fluid is incompressible; more precisely, its total density and the densities of each component are constant. Therefore, this model is restricted to the density matched case and cannot be used for the case where the two incompressible fluids have different densities. To treat problems with small density ratios, a Boussinesq approximation is often used, where the small density difference is neglected except in the gravitational force. The model achieved maintains thermodynamic consistency (see, for example, Hua *et al.* 2011). This approach, however, is no longer valid for large density ratios. Several generalizations of model H for the case of different densities have been presented and discussed by Lowengrub & Truskinovsky (1998), Boyer (2002), Ding *et al.* (2007), Shen & Yang (2010) and most recently by Abels, Garcke & Grün (2012). Thermodynamic consistency, however, could only be shown for the models proposed by Lowengrub & Truskinovsky (1998) and Abels *et al.* (2012). Benchmark computations for three of them, namely the models of Boyer (2002), Ding *et al.* (2007) and Abels *et al.* (2012), were carried out by Aland & Voigt (2012). Moreover, several works have been performed to study the model of Abels *et al.* (2012). Grun & Klingbeil (2014) presented a numerical method, where the mixed finite element formulation was employed in order that the discrete energy law of the numerical method could be obtained. The convergence of the method was presented in Grun (2013). Garcke, Hinze & Kahle (2014) presented a numerical method that satisfied

an energy inequality. Antanovskii (1995) derived a quasi-incompressible phase-field model for two-phase flow with different densities. The extended model was presented by Lowengrub & Truskinovsky (1998), where the pressure rather than the density was employed as an independent variable, and worked through the Gibbs free energy. In their model, the two fluids of different densities are assumed to be mixed and compressible along the interfacial region (introducing quasi-incompressibility into the model). The flow in the interfacial region is in general non-solenoidal ($\nabla \cdot \mathbf{v} \neq 0$), resulting in an expansion or contraction flow. Thermodynamic consistency is maintained within the resulting system (quasi-incompressible NSCH), where the Navier–Stokes equations are coupled with the Cahn–Hilliard equations, and the kinetic fluid pressure and variable density are introduced into the chemical potential. Very recently, a numerical method for the quasi-incompressible NSCH system with a discrete thermodynamic law (energy law) was presented by Guo *et al.* (2014a), where the quasi-incompressibility (the non-solenoidal velocity) near interfaces was captured. Namely, the numerical results reveal that away from interfaces the fluid is incompressible, while near interfaces waves of expansion and contraction are observed. Very recently, another model of quasi-incompressible fluids for phase transition simulation was developed by Giesselmann & Pryer (2013), where a discontinuous Galerkin finite element method was used and studied in Aki *et al.* (2014). The model considered differs from the quasi-incompressible NSCH system developed in Lowengrub & Truskinovsky (1998) in that the volume fraction, rather than the mass concentration, is used as the phase variable. In addition, the two models are derived with different energy functionals.

Another assumption for model H is that the fluid flow is isothermal. However, for the case that considers thermocapillary (Marangoni) effects, the surface tension gradient is produced by the non-uniform distribution of the temperature, so that the system cannot be assumed to be isothermal and the transport of the temperature field cannot be ignored. The extension of model H in the non-isothermal case was presented by Jasnow & Vinals (1996), where, to study the thermocapillary motion of droplets, a constant externally imposed temperature gradient was considered. Several other works, as mentioned above, have also been devoted to the use of the phase-field method to simulate the dynamics of an interface with thermocapillary effects (Borcia & Besthorn 2003; Borcia *et al.* 2004; Sun *et al.* 2009; Guo *et al.* 2014b). For most of these models, the system equations of the flow field (the Navier–Stokes equations with extra stress) and phase field (the advective Cahn–Hilliard equations) are usually derived from the free energy functional that depends on temperature. The energy equations, however, are not derived together with the system equations. Instead, either the classical energy transport equations are incorporated into the system directly, or the temperature fields are fixed and the energy equations are not needed. Therefore, thermodynamic consistency can hardly be maintained. It turns out that the concept of thermodynamic consistency plays an important role in phase-field modelling. As the phase-field model can be derived through variational procedures, thermodynamic consistency of the model equations can serve as a justification of the model. In addition, it ensures that the model is compatible with the laws of thermodynamics, and that it has a strict relaxational behaviour of the free energy; hence the models are more than a phenomenological description of an interfacial problem. Antanovskii (1995) presented a phase-field model to study the thermocapillary flow in a gap, where to obtain a free energy that depended on the temperature, the Cahn–Hilliard gradient term associated with the phase field was introduced into the entropy functional of the system, which led to a corresponding extra term appearing in the energy equation.

The resulting system of equations was derived together through the local balance laws and thermodynamic relations, which maintained thermodynamic consistency. A similar gradient entropy term was considered by Anderson & McFadden (1996) to study a single compressible fluid with different phases near its critical point. In their work, the phase-field model was derived through a thermodynamic formalism (Sekerka 1993) based on entropy generation. Through a similar thermodynamic framework, Verschueren, van de Vosse & Meijer (2001) presented a phase-field model for two-phase flow with thermocapillary effects in a Hele-Shaw cell. The system of equations maintained thermodynamic consistency, in which the energy equation contained an extra term associated with the variations of the phase field.

In the present paper, we develop a thermodynamically consistent phase-field model for two-phase flows with thermocapillary effects, which allows the binary incompressible fluid (quasi-incompressible fluid) to have different densities, viscosities and thermal conductivities for each component. By employing the thermodynamic framework used by Anderson & McFadden (1996), we first derive a phase-field model for binary compressible flows with thermocapillary effects, where the mass concentration is chosen as the phase variable to label the phases, and the Helmholtz free energy is chosen as the fluid free energy. We then derive the model for binary incompressible flows with thermocapillary effects. Following the work of Lowengrub & Truskinovsky (1998), we employ the pressure rather than the density as the independent variable and thus work with the Gibbs free energy. The equations of both models, including the Navier–Stokes equations with extra stress, an advective Cahn–Hilliard equation and an energy equation, are derived under a thermodynamic framework. To the best of our knowledge, such a thermodynamically consistent phase-field model for binary incompressible fluid with thermocapillary effects, which allows for different physical properties of each component, is new. To validate our model, we first show that thermodynamic consistency is maintained in both models, where the first and second laws of thermodynamics are derived from the model equations. We also show that the system equations of our model satisfy Onsager’s reciprocal relation and Galilean invariance, which can be critical for phase-field modelling. We then analyse the model in the sharp-interface limit to show that the governing equations and interfacial conditions of the classical sharp-interface model can be recovered from our phase-field models. This further reveals the underlying physical mechanisms of the phase-field model. In the jump condition of momentum balance, we relate the surface tension term of our phase-field model to that of the classical sharp-interface model by introducing a ratio parameter, where the value of the parameter can be determined through the provided relation. As another validation of our model, three examples are computed by using a continuous finite element method, including thermocapillary convection in two-layer fluid system and thermocapillary migration of a drop in a medium fluid. The numerical results for the first two examples are consistent with the corresponding analytical solutions (Pendse & Esmaeeli 2010) and the existing numerical solutions (Herrmann *et al.* 2008). It should be noted that for all the examples computed in this paper, we assume that the interface has no contact with the boundary of the domain. In the case that the interface contacts the boundary of the domain, extra difficulties would arise from complicated interface/boundary interacting conditions and should be dealt with separately (e.g. Qian *et al.* 2006; Eck *et al.* 2009; Gao & Wang 2012).

The paper is organized as follows. In § 2, we introduce the variable density and mass-averaged velocity of the binary fluid. We then present the derivations of the phase-field model for binary compressible fluid with thermocapillary effects in § 3, and

the corresponding derivations for binary incompressible (quasi-incompressible) fluid in §4. The sharp-interface limit analysis of our phase-field model is carried out in §5. Section 6 shows some numerical results as validations of our model. Finally, the conclusion and future work are discussed in §7.

2. Variable density and mass-averaged velocity

In phase-field modelling, an order parameter (phase variable) is normally introduced to distinguish different phases and the intervening interface. Lowengrub & Truskinovsky (1998) have argued for the advantage of using a physically realistic scalar field instead of an artificial smoothing function for the interface. Several physically realistic scalar fields have been suggested as the order parameters for phase-field modelling, e.g. the mass density ρ for the case of a single compressible fluid with different phases (Anderson & McFadden 1996), the mass concentration c of one of the constituents for the case of compressible and incompressible binary fluid (Lowengrub & Truskinovsky 1998; Abels *et al.* 2012) or an alternative phase variable, the volume fraction ϕ , for the case of incompressible binary fluid (Liu & Shen 2002) and solidification of single materials (Wang *et al.* 1993). Here, we choose the mass concentration c of one of the constituents as the phase variable, and begin by introducing the variable density of the mixture. We consider a mixture of two fluids in a domain Ω , and take a sufficient small material volume $V \in \Omega$. We then have the following theorem (e.g. Mase & Mase 1999).

THEOREM 1. *For a smooth function $f(\mathbf{x}, t)$ in the Eulerian coordinate,*

$$\frac{d}{dt} \int_{V(t)} f(\mathbf{x}, t) dV = \int_{V(t)} \left(\frac{Df}{Dt} + f(\nabla \cdot \mathbf{v}) \right) dV = \int_{V(t)} \left(\frac{\partial f}{\partial t} + \nabla \cdot (f\mathbf{v}) \right) dV, \quad (2.1)$$

where $D/Dt = \partial/\partial t + \mathbf{v} \cdot \nabla$ is the material derivative and \mathbf{v} is the velocity of the moving volume $V(t)$.

In the control volume, the two fluids are labelled by $i = 1, 2$ and they fill the volumes V_i separately. We then introduce the volume fraction γ_i for the i th fluid such that $\gamma_i = V_i/V$. Further, we assume that two fluids can mix along the interfacial region and the volume occupied by a given amount of mass of the single fluid does not change after mixing. Then, within the material volume V , the γ_i satisfy the condition $\gamma_1 + \gamma_2 = 1$. Let $M = M_1 + M_2$ be the total mass of the mixture, and M_i be the mass of the i th fluid in the volume. We now introduce the local volume-averaged mass density taken over the sufficient small volume V for each fluid $\tilde{\rho}_i = M_i/V$, and the actual local mass density for each fluid $\rho_i = M_i/V_i$. It should be noted that for incompressible components, we assume that the ρ_i are uniform constants. Having in mind the definition of volume fraction, we obtain the relation between the volume-averaged mass densities and the local mass densities,

$$\gamma_i = \frac{\tilde{\rho}_i}{\rho_i} \quad \text{and} \quad \frac{\tilde{\rho}_1}{\rho_1} + \frac{\tilde{\rho}_2}{\rho_2} = 1. \quad (2.2a,b)$$

We then define the volume-averaged mass density for the mixture as

$$\rho = \tilde{\rho}_1 + \tilde{\rho}_2 = \frac{M_1 + M_2}{V} = \frac{M}{V}. \quad (2.3)$$

Let c_i be the mass concentration for the i th fluid, such that

$$c_i = \frac{M_i}{M} = \frac{\tilde{\rho}_i}{\rho} \quad \text{and} \quad c_1 + c_2 = 1. \quad (2.4a,b)$$

Using (2.2) and (2.4), we obtain the variable density for the mixture of two fluids,

$$\frac{1}{\rho(c)} = \frac{c}{\rho_1} + \frac{1-c}{\rho_2}. \quad (2.5)$$

Here, we chose the mass concentration of fluid 1 as the phase variable for our phase-field model, such that $c = c_1 = 1 - c_2$. It can be seen that, for two incompressible components of different densities, the variable density $\rho(c)$ for the mixture is constant almost everywhere except near the interfacial region. For simplicity, we write the variable density $\rho(c)$ as ρ in all the following derivations.

Now we suppose that the two fluids move with different velocities $\mathbf{v}_i(\mathbf{x}, t)$. The equation of mass balance for each fluid within the material volume V can then be written in the form (Lowengrub & Truskinovsky 1998; Boyer 2002; Abels *et al.* 2012)

$$\frac{\partial \tilde{\rho}_i}{\partial t} + \nabla \cdot (\tilde{\rho}_i \mathbf{v}_i) = 0. \quad (2.6)$$

We then introduce the mass-averaged velocity for the mixture as

$$\rho \mathbf{v} = \tilde{\rho}_1 \mathbf{v}_1 + \tilde{\rho}_2 \mathbf{v}_2 \quad \text{or} \quad \mathbf{v} = c_1 \mathbf{v}_1 + c_2 \mathbf{v}_2. \quad (2.7a,b)$$

Substituting the density (2.3) and mass-averaged velocity (2.7) into (2.6), we obtain the mass balance for the mixture of two fluids,

$$\frac{\partial \rho}{\partial t} + \nabla \cdot (\rho \mathbf{v}) = 0. \quad (2.8)$$

In the following derivations, we consider the mixture as a single fluid moving with velocity \mathbf{v} . It should be noted that if we consider a binary incompressible fluid (assuming that the two fluids of the mixture are incompressible, and that the temperature effects on the densities of both fluids are negligible), then ρ_1 and ρ_2 are constants, and the above (2.8) can be further written as

$$\nabla \cdot \mathbf{v} = -\frac{1}{\rho} \frac{D\rho}{Dt} = -\frac{1}{\rho} \frac{d\rho}{dc} \frac{Dc}{Dt} = \alpha \rho \frac{Dc}{Dt}, \quad (2.9)$$

where $\alpha = (\rho_2 - \rho_1)/\rho_2\rho_1$ is constant. We note that, due to the variations of the phase variable c , the mass-averaged velocity for the mixture is non-solenoidal ($\nabla \cdot \mathbf{v} \neq 0$) near the interfacial region, which introduces compressibility effects into the model. Such a binary incompressible fluid is termed as a quasi-incompressible fluid (e.g. Antanovskii 1995, Lowengrub & Truskinovsky 1998).

We remark that apart from this mass-averaged velocity \mathbf{v} , another velocity for the mixture, the volume-averaged velocity $\tilde{\mathbf{v}}$, was considered by Abels *et al.* (2012), Boyer (2002) and Ding *et al.* (2007), where the volume fraction γ instead of the mass concentration c was employed as the phase variable, and further used to relate the velocities of the single fluids and mixture. This volume-averaged velocity of binary incompressible fluid is solenoidal ($\nabla \cdot \tilde{\mathbf{v}} = 0$) over the whole domain, where

an extra term that accounts for the mass flux relative to the volume-averaged velocity appears in the Navier–Stokes equations (see, for details, Abels *et al.* 2012).

3. Phase-field model for binary compressible fluid with thermocapillary effects

In this section, we develop a system of equations for a binary fluid with thermocapillary effects, in which both components are compressible and Cahn–Hilliard diffusion is coupled with fluid motion.

3.1. Derivation of the model

We first consider a mixture of two fluids in a domain Ω , and we take an arbitrary material volume $V \in \Omega$ that moves with the mixture. Within the material volume, we define the properties of the binary compressible fluid as

$$M = \int_{V(t)} \rho dV, \tag{3.1}$$

$$\mathbf{P} = \int_{V(t)} \rho \mathbf{v} dV, \tag{3.2}$$

$$E = \int_{V(t)} \left(\frac{1}{2} \rho |\mathbf{v}|^2 + \rho gz + \rho \hat{u} \right) dV, \tag{3.3}$$

$$S = \int_{V(t)} \rho \hat{s} dV, \tag{3.4}$$

$$C = \int_{V(t)} \rho c dV, \tag{3.5}$$

where M , \mathbf{P} , E and S are the total mass, momentum, energy and entropy of the mixture, $\rho(c)$ is the variable density of the mixture, \mathbf{v} is the mass-averaged velocity of the mixture, $|\mathbf{v}|^2/2$ is the kinetic energy per unit mass, gz is the gravitational potential energy per unit mass, z is the z -coordinate, \hat{u} (\hat{s}) is the internal energy (entropy) per unit mass and c is the phase variable. Substitution of the mass concentration (2.4) into (3.5) gives

$$C = \int_{V(t)} \rho c dV = \int_{V(t)} \rho c_1 dV = \int_{V(t)} \tilde{\rho}_1 dV, \tag{3.6}$$

where C stands for the constituent mass of fluid 1 within the material volume $V(t)$. In phase-field modelling, apart from the classical free energy density for bulk phases, an extra gradient term is typically added into the model to account for the free energy of the diffuse interface (Cahn & Hilliard 1958). Several ways have been suggested to introduce the gradient term into the phase-field model, e.g. by introducing it into the entropy functional (Wang *et al.* 1993; Antanovskii 1995), free energy functional (Lowengrub & Truskinovsky 1998) or internal energy functional (Anderson *et al.* 1998; Verschueren *et al.* 2001). In the present work, as the thermocapillary effects along the interface are investigated, we expect the surface free energy (serving as the surface tension (see § 5.4)) of our phase-field model to be temperature-dependent. Therefore, according to the thermodynamic relations, we introduce the gradient term

into both the internal energy and the entropy of our model, such that

$$\hat{u}(s, \rho, c, \nabla c) = u(s, \rho, c) + u^{grad}(\nabla c), \quad u^{grad} = \lambda_u \frac{1}{2} |\nabla c|^2, \quad (3.7)$$

$$\hat{s}(T, \rho, c, \nabla c) = s(T, \rho, c) + s^{grad}(\nabla c), \quad s^{grad} = \lambda_s \frac{1}{2} |\nabla c|^2, \quad (3.8)$$

$$\hat{f}(T, \rho, c, \nabla c) = f(T, \rho, c) + f^{grad}(T, \nabla c), \quad f^{grad} = \lambda_f(T) \frac{1}{2} |\nabla c|^2, \quad (3.9)$$

where u , s and f stand for the classical parts of the specific internal energy, entropy and free energy separately. Here, f is the Helmholtz free energy. The parts u^{grad} , s^{grad} and f^{grad} are the gradient terms analogous to the Landau–Ginzburg (Ginzburg & Landau 1950) or Cahn–Hilliard (Cahn & Hilliard 1958) gradient energy. It should be noted that these parts are termed as the ‘non-classical’ terms by Anderson & McFadden (1996), who used a phase-field model to study a single compressible fluid with different phases near its critical point. In addition, λ_u and λ_s are constant parameters, and $\lambda_f(T)$ is a parameter depending on the temperature and will lead to thermocapillary effects along the interface. It should be noted that λ_u , λ_s and $\lambda_f(T)$ can be further used to relate the surface tension of the phase-field model to that of the sharp-interface model when the phase-field model reduces to its sharp-interface limit (see § 5.4 for details). As $u(\rho, s, c)$ is the classical contribution to the specific internal energy \hat{u} , we have the thermodynamic relation

$$du(s, \rho, c) = \left. \frac{\partial u}{\partial s} \right|_{\rho, c} ds + \left. \frac{\partial u}{\partial \rho} \right|_{s, c} d\rho + \left. \frac{\partial u}{\partial c} \right|_{s, \rho} dc = Tds + \frac{p}{\rho^2} d\rho + \left. \frac{\partial u}{\partial c} \right|_{s, \rho} dc, \quad (3.10)$$

where the subscripts indicate which variables are held constant when the various partial derivatives are taken. This relation states that the heat transfer (Tds), pressure–volume work ($p/\rho^2 d\rho$) and chemical work ($(\partial u/\partial c)dc$) all contribute to the changes in the internal energy. Further, we have the thermodynamic relation for the Helmholtz free energy,

$$f = u - Ts. \quad (3.11)$$

Having in mind the relation (3.10), we obtain

$$df = du - d(Ts) = du - sdT - Tds = \frac{p}{\rho^2} d\rho - sdT + \left. \frac{\partial u}{\partial c} \right|_{s, \rho} dc, \quad (3.12)$$

such that

$$\left. \frac{\partial f}{\partial \rho} \right|_{T, c} = \frac{p}{\rho^2}, \quad \left. \frac{\partial f}{\partial T} \right|_{\rho, c} = -s \quad \text{and} \quad \left. \frac{\partial f}{\partial c} \right|_{T, \rho} = \left. \frac{\partial u}{\partial c} \right|_{s, \rho}. \quad (3.13a, b)$$

Similarly, we assume that the same thermodynamic relations that hold for the classical terms also hold for the general terms, such that

$$\hat{f} = \hat{u} - T\hat{s} \quad \text{and} \quad \left. \frac{\partial \hat{f}}{\partial T} \right|_{s, \rho, c, \nabla c} = -\hat{s}. \quad (3.14a, b)$$

With the relations (3.11) and (3.13), we must also have the relations for the gradient terms,

$$f^{grad} = u^{grad} - Ts^{grad} \quad \text{and} \quad \left. \frac{\partial f^{grad}}{\partial T} \right|_{\nabla c} = -s^{grad}, \quad (3.15a, b)$$

and for the corresponding coefficients,

$$\lambda_f(T) = \lambda_u - T\lambda_s \quad \text{and} \quad \frac{d\lambda_f(T)}{dT} = -\lambda_s. \tag{3.16a,b}$$

For simplicity, we omit all the subscripts in the following derivations. Under the assumptions above, the general forms of the physical balance associated with M , \mathbf{P} , E , S and C can be given as follows:

$$\frac{dM}{dt} = 0, \tag{3.17}$$

$$\frac{d\mathbf{P}}{dt} = \int_{\partial V(t)} \mathbf{m} \cdot \hat{\mathbf{n}} dA - \int_{V(t)} \rho g \hat{\mathbf{z}} dV, \tag{3.18}$$

$$\frac{dE}{dt} = \int_{\partial V(t)} (\mathbf{v} \cdot \mathbf{m} \cdot \hat{\mathbf{n}} - \mathbf{q}_E \cdot \hat{\mathbf{n}} - \mathbf{q}_E^{nc} \cdot \hat{\mathbf{n}}) dA, \tag{3.19}$$

$$\frac{dS}{dt} = - \int_{\partial V(t)} \left(\frac{\mathbf{q}_E}{T} \cdot \hat{\mathbf{n}} + \mathbf{q}_S^{nc} \cdot \hat{\mathbf{n}} \right) dA + \int_{V(t)} S_{gen} dV \quad (S_{gen} \geq 0), \tag{3.20}$$

$$\frac{dC}{dt} = - \int_{\partial V(t)} \mathbf{q}_C \cdot \hat{\mathbf{n}} dA, \tag{3.21}$$

where $\hat{\mathbf{n}}$ is the unit outward normal vector of the boundary and $\hat{\mathbf{z}}$ is the vertical component of the unit normal vector. Equation (3.17) represents the mass balance of the mixture within the volume. Equation (3.18) represents the momentum balance, stating that the rate of change in total momentum equals the force (surface forces \mathbf{m} and body forces $\rho g \hat{\mathbf{z}}$) acting on the volume. Here, only the gravitational forces are considered. The energy balance equation (3.19) states that the change in total energy equals the rate of work done by the forces (\mathbf{m}) on the boundary plus the energy flux (classical \mathbf{q}_E and non-classical \mathbf{q}_E^{nc} internal energy flux) through the boundary. The entropy balance (3.20) states that the rate of change of entropy in the control volume during the process equals the net entropy transfer through the boundary (classical \mathbf{q}_E/T and non-classical \mathbf{q}_S^{nc} entropy flux) plus the local entropy generation ($S_{gen} \geq 0$) within the control volume (e.g. Moran *et al.* 2010). Based on the second law of thermodynamics, the local entropy generation is non-negative for a dissipative system (or, say, for an irreversible process), which is key to the thermodynamic frame that we used for the derivations. For the constituent mass balance (3.21), we use (3.6) and Theorem 1 to obtain

$$\frac{dC}{dt} = \frac{d}{dt} \int_{V(t)} \tilde{\rho}_1 dV = \int_{V(t)} \left(\frac{\partial \tilde{\rho}_1}{\partial t} + \nabla \cdot (\tilde{\rho}_1 \mathbf{v}) \right) dV = - \int_{\partial V(t)} \mathbf{q}_C \cdot \hat{\mathbf{n}} dA. \tag{3.22}$$

Substituting (2.6) into (3.22), we obtain $\mathbf{q}_C = \tilde{\rho}_1(\mathbf{v}_1 - \mathbf{v})$, where \mathbf{q}_C stands for the mass flux of fluid 1 with velocity $(\mathbf{v}_1 - \mathbf{v})$ through the boundary of the control volume. It should be noted that in the following derivations \mathbf{q}_C will be related to the chemical potential of the phase field, which is analogous to the standard derivations of the Cahn–Hilliard equations (see, for example, Anderson *et al.* 1998; Lowengrub & Truskinovsky 1998).

In what follows, we use the definitions (3.1)–(3.5) and the balance laws (3.17)–(3.21) to obtain equations that are expressed in terms of the above unknowns, including \mathbf{m} , \mathbf{q}_E , \mathbf{q}_E^{nc} , \mathbf{q}_S^{nc} , \mathbf{q}_C and S_{gen} . We then specify these unknowns with respect

to the second law of thermodynamics (ensuring $S_{gen} \geq 0$) and the concept of thermodynamic consistency of the phase-field model.

For the mass balance (3.17), we use Theorem 1 to obtain

$$\frac{D\rho}{Dt} = -\rho(\nabla \cdot \mathbf{v}), \tag{3.23}$$

based on which we have the following.

THEOREM 2 (Transport Theorem 2). *For a smooth function $f(\mathbf{x}, t)$ in the Eulerian coordinate,*

$$\frac{d}{dt} \int_{V(t)} \rho f(\mathbf{x}, t) dV = \int_{V(t)} \rho \frac{Df}{Dt} dV = \int_{V(t)} \rho \left(\frac{\partial f}{\partial t} + (\mathbf{v} \cdot \nabla) f \right) dV, \tag{3.24}$$

where ρ is the density of the mixture defined in the volume $V(t)$ and satisfies the mass balance (3.23).

It should be noted that as Theorems 1 and 2 are frequently used, we will not refer to them in the following derivations.

For momentum balance (3.18), we simply have

$$\rho \frac{D\mathbf{v}}{Dt} = \nabla \cdot \mathbf{m} - \rho g \hat{\mathbf{z}}. \tag{3.25}$$

For energy balance (3.19), we obtain

$$\begin{aligned} \rho T \frac{Ds}{Dt} = & -\nabla \cdot \left(\rho \lambda_u \frac{Dc}{Dt} \nabla c \right) + (\mathbf{m} - \rho \lambda_u |\nabla c|^2 \mathbf{I} + \rho \lambda_u (\nabla c \otimes \nabla c)) : \nabla \mathbf{v} \\ & + \lambda_u \rho \Delta c \frac{Dc}{Dt} - \nabla \cdot \mathbf{q}_E - \nabla \cdot \mathbf{q}_E^{nc} - \rho \frac{\partial u}{\partial c} \frac{Dc}{Dt} - \frac{p}{\rho} \frac{D\rho}{Dt}, \end{aligned} \tag{3.26}$$

where (3.10), (3.23) and (3.25) and the following identities are used:

$$\frac{d}{dt} \int_{V(t)} \rho g z dV = \int_{V(t)} \rho g \mathbf{v} \cdot \nabla z dV = \int_{V(t)} \rho g \mathbf{v} \cdot \hat{\mathbf{z}} dV \tag{3.27}$$

and

$$\begin{aligned} \rho \frac{D}{Dt} \left(\frac{1}{2} \lambda_u |\nabla c|^2 \right) = & \nabla \cdot \left(\rho \lambda_u \frac{Dc}{Dt} \nabla c \right) \\ & + (\rho \lambda_u |\nabla c|^2 \mathbf{I} - \rho \lambda_u (\nabla c \otimes \nabla c)) : \nabla \mathbf{v} - \rho \lambda_u \Delta c \frac{Dc}{Dt}. \end{aligned} \tag{3.28}$$

Here, ‘:’ stands for the double dot product of the stress tensor (e.g. Mase & Mase 1999).

For entropy balance (3.20), we obtain

$$\begin{aligned} \rho \frac{Ds}{Dt} = & -\nabla \cdot \left(\rho \lambda_s \frac{Dc}{Dt} \nabla c \right) + (-\rho \lambda_s |\nabla c|^2 \mathbf{I} + \rho \lambda_s (\nabla c \otimes \nabla c)) : \nabla \mathbf{v} \\ & + \lambda_s \rho \Delta c \frac{Dc}{Dt} - \nabla \cdot \left(\frac{\mathbf{q}_E}{T} \right) + S_{gen} - \nabla \cdot \mathbf{q}_S^{nc}, \end{aligned} \tag{3.29}$$

where, similarly to (3.28), the following identity is used:

$$\rho \frac{D}{Dt} \left(\frac{1}{2} \lambda_s |\nabla c|^2 \right) = \nabla \cdot \left(\rho \lambda_s \frac{Dc}{Dt} \nabla c \right) + (\rho \lambda_s |\nabla c|^2 \mathbf{I} - \rho \lambda_s (\nabla c \otimes \nabla c)) : \nabla \mathbf{v} - \rho \lambda_s \Delta c \frac{Dc}{Dt}. \quad (3.30)$$

For constituent mass balance (3.21), we simply have

$$\rho \frac{Dc}{Dt} = -\nabla \cdot \mathbf{q}_C. \quad (3.31)$$

We then use (3.29) and (3.31) to substitute the terms $\rho Ds/Dt$ and $\rho Dc/Dt$ in (3.26), and use the relation (3.16) to obtain the expression for the entropy generation,

$$\begin{aligned} S_{gen} &= \frac{1}{T} (\mathbf{m} - \rho \lambda_f(T) |\nabla c|^2 \mathbf{I} + \rho \lambda_f(T) \mathbf{T} + p \mathbf{I}) : \nabla \mathbf{v} \\ &+ \nabla \cdot \frac{1}{T} \cdot \left(\rho \lambda_u \frac{Dc}{Dt} \nabla c + \mathbf{q}_E + \mathbf{q}_E^{nc} - \mu_C \mathbf{q}_C \right) \\ &- \nabla \cdot \left[\frac{1}{T} \rho \lambda_f(T) \frac{Dc}{Dt} \nabla c + \frac{1}{T} \mathbf{q}_E^{nc} - \frac{1}{T} \mu_C \mathbf{q}_C - \mathbf{q}_S^{nc} \right] - \frac{1}{T} \mathbf{q}_C \cdot \nabla \mu. \end{aligned} \quad (3.32)$$

To ensure the non-negativity of the entropy generation $S_{gen} \geq 0$ (second law of thermodynamics), we specify the unknown terms in the form

$$\mathbf{q}_E = -k(c) \nabla T, \quad \mathbf{q}_E^{nc} = -\rho \lambda_u \frac{Dc}{Dt} \nabla c + \mu_C \mathbf{q}_C, \quad (3.33)$$

$$\mathbf{q}_S^{nc} = -\rho \lambda_s \frac{Dc}{Dt} \nabla c, \quad \mathbf{m} = \rho \lambda_f(T) |\nabla c|^2 \mathbf{I} - \rho \lambda_f(T) \mathbf{T} + \boldsymbol{\sigma}, \quad (3.34)$$

$$\mu_C = \frac{\partial f}{\partial c} - \lambda_f(T) \Delta c, \quad \mathbf{q}_C = -m_C \nabla \mu_C, \quad (3.35)$$

$$\mathbf{T} = \nabla c \otimes \nabla c, \quad \boldsymbol{\sigma} = -p \mathbf{I} + \boldsymbol{\tau}, \quad (3.36)$$

$$p = \rho^2 \frac{\partial f}{\partial \rho}, \quad \boldsymbol{\tau} = \mu(c) (\nabla \mathbf{v} + \nabla \mathbf{v}^T) - \frac{2}{3} \mu(c) (\nabla \cdot \mathbf{v}) \mathbf{I}. \quad (3.37)$$

It should be noted that $\boldsymbol{\tau}$ is the deviatoric stress tensor from the classical Navier–Stokes equations (e.g. Batchelor 2000). Here, we use the thermodynamic relation (3.13) to obtain the chemical potential μ_C . The pressure p can be obtained immediately through the thermodynamic relation (3.13). By substituting the above terms into (3.17)–(3.21), we obtain the system of equations for the phase-field model governing binary compressible flows with thermocapillary effects,

$$\frac{D\rho}{Dt} = -\rho (\nabla \cdot \mathbf{v}), \quad (3.38)$$

$$\rho \frac{D\mathbf{v}}{Dt} = \nabla \cdot \mathbf{m} - \rho g \hat{\mathbf{z}}, \quad (3.39)$$

$$\begin{aligned} \rho \frac{Du}{Dt} &= (\boldsymbol{\sigma} - \rho T \lambda_s |\nabla c|^2 \mathbf{I} + \rho T \lambda_s \mathbf{T}) : \nabla \mathbf{v} + \lambda_u \nabla \cdot (\rho \nabla c) \frac{Dc}{Dt} \\ &+ \nabla \cdot (k(c) \nabla T + m_C \mu_C \nabla \mu_C), \end{aligned} \quad (3.40)$$

$$\rho \frac{Ds}{Dt} = \frac{1}{T} (\boldsymbol{\tau} - \rho T \lambda_s |\nabla c|^2 \mathbf{I} + \rho T \lambda_s \mathbf{T}) : \nabla \mathbf{v} + \lambda_s \nabla \cdot (\rho \nabla c) \frac{Dc}{Dt} + \frac{1}{T} \nabla \cdot (k(c) \nabla T), \quad (3.41)$$

$$\rho \frac{Dc}{Dt} = m_c \Delta \mu_c, \quad (3.42)$$

$$\mu_c = \frac{\partial f}{\partial c} - \lambda_f(T) \Delta c. \quad (3.43)$$

It should be noted that the second term in the stress tensor \mathbf{m} is the extra reactive stress (Ericksen's stress) to mimic the surface tension. This stress term is associated with the presence of concentration gradient energy (Cahn–Hilliard energy). We note that the temperature-dependent coefficient in \mathbf{m} is a linear function of temperature, which leads to thermocapillary effects along the interface (see §4.2 for details). Here, m_c is a positive constant standing for the mobility of the diffuse interface. It should be noted that in the non-classical heat (or entropy) flux \mathbf{q}_E^{nc} (or \mathbf{q}_S^{nc}), the term $\rho \lambda_u \nabla c Dc/Dt$ (or $\rho \lambda_s \nabla c Dc/Dt$) is associated with the gradient energy (or entropy respectively) and is in the direction of the gradient of the phase variable. Similar terms were obtained by Wang *et al.* (1993), who used a phase-field model to study the solidification of single material, and by Anderson & McFadden (1996), who used a phase-field model to study a single compressible fluid with different phases near its critical point. In addition, a non-classical energy flux term $m_c \mu_c \nabla \mu_c$ appears in our energy balance equation (3.40). The same energy flux term was obtained by Gurtin *et al.* (1996) (see (28)), who re-derived the model H in the framework of classical continuum mechanics. A 'counterpart' entropy flux term was identified by Lowengrub & Truskinovsky (1998) when deriving a phase-field model for binary compressible fluid, where this term is required to keep the model compatible with the second law of thermodynamics. In the latter work, the isothermal fluid flow was studied, so that the temperature T in the entropy flux was treated as constant, whereas in our work, the temperature is not a constant as the thermocapillary effects are considered here. They identified this non-classical term as the entropy flux transported through the boundary by chemical diffusion. Our model agrees with these works well and therefore we identify this non-classical energy flux term as the energy that is carried into the control volume by the chemical diffusion. It should be noted that several phase-field models (e.g. Blesgen 1999; Allaire, Clerc & Kokh 2002; Abels & Feireisl 2008) have been presented to study binary compressible fluids, where the specifications of the free energy (3.37) that contributes to the compressibility of binary compressible fluids are discussed and provided.

Similarly to the approach that defines the variable density $\rho(c)$ (2.5), we define the variable viscosity $\mu(c)$ and the variable thermal diffusivity $k(c)$ for the mixture in the form of the harmonic average,

$$\mu(c) = \frac{\mu_1 \mu_2}{(\mu_2 - \mu_1)c + \mu_1}, \quad k(c) = \frac{k_1 k_2}{(k_2 - k_1)c + k_1}, \quad (3.44a,b)$$

where μ_i and k_i are the viscosity and thermal conductivity of the i th fluid.

3.2. Thermodynamic consistency and Galilean invariance

As our phase-field model (3.38)–(3.43) is derived within a thermodynamic framework, it implies that the first and second thermodynamic laws are naturally underlying

the model. However, from the numerical point of view, thermodynamic consistency can further serve as a criterion to design the numerical methods. In our phase-field model, the Navier–Stokes equations are coupled with the Cahn–Hilliard equations and energy balance equation, which leads to a nonlinear system. Moreover, as rapid variations in the solutions of the phase variable occur near the interfacial region, the energy stability of the numerical method is critical. Recently, the preservation of the thermodynamic laws at the discrete level has been reported to play an important role in the design of numerical methods (e.g. Lin & Liu 2006; Lin, Liu & Zhang 2007 for liquid crystal models; Hua *et al.* 2011; Guo *et al.* 2014a for phase-field models), which not only immediately implies the stability of the numerical scheme, but also ensures the correctness of the solutions. Hence, in contrast to the derivations, we now show that the first and second laws of thermodynamics can be derived from the system of (3.38)–(3.43), which can be further used to design the numerical methods. In addition, important modelling properties, Onsager reciprocal relations and Galilean invariance will be verified as well.

3.2.1. The laws of thermodynamics

By multiplying (3.38), (3.39) and (3.41)–(3.43) by $p/\rho + \mathbf{v} \cdot \mathbf{v}/2 + u$, \mathbf{v} , T , μ_C and $\rho Dc/Dt$, and summing them up, we can obtain the first law of thermodynamics (3.19) that we used to derive the model. By substituting the terms \mathbf{m} , \mathbf{q}_E , \mathbf{q}_E^{nc} , \mathbf{q}_S^{nc} and \mathbf{q}_C into the entropy generation (3.32), we obtain the second law of thermodynamics,

$$\begin{aligned} S_{gen} &= \frac{1}{T} \boldsymbol{\tau} : \nabla \mathbf{v} - \mathbf{q}_E \frac{\nabla T}{T^2} - \mathbf{q}_C \frac{1}{T} \nabla \mu_C \\ &= \frac{1}{T} \boldsymbol{\tau} : \nabla \mathbf{v} + k(c) \left| \frac{\nabla T}{T} \right|^2 + \frac{m_C}{T} |\nabla \mu_C|^2 \geq 0, \end{aligned} \tag{3.45}$$

where we see that the viscous dissipation, heat transfer and chemical potential (the variation of the phase variable) all contribute to the entropy generation of our phase-field model. It should be noted that the same entropy generation equation was obtained by Lowengrub & Truskinovsky (1998) when deriving the phase-field model for binary compressible fluid.

3.2.2. Onsager reciprocal relations

From (3.45), we observe that the entropy generation can be seen as the sum of terms, each being a product of a flux ($\boldsymbol{\tau}$, \mathbf{q}_E , \mathbf{q}_C) and thermodynamic forces ($\nabla \mathbf{v}$, ∇T , $\nabla \mu_C$). The simplest model, based on the linear thermodynamics of non-equilibrium processes (Groot & Mazur 1985), assumes linear relations between the fluxes and thermodynamic forces, such that

$$\boldsymbol{\tau} = L_{11} \nabla \mathbf{v} + L_{12} \nabla T + L_{13} \nabla \mu_C, \tag{3.46}$$

$$\mathbf{q}_E = L_{21} \nabla \mathbf{v} + L_{22} \nabla T + L_{23} \nabla \mu_C, \tag{3.47}$$

$$\mathbf{q}_C = L_{31} \nabla \mathbf{v} + L_{32} \nabla T + L_{33} \nabla \mu_C, \tag{3.48}$$

where the coefficients L_{ij} are chosen to guarantee the non-negativity of S_{gen} . Moreover, microscopic reversibility requires the Onsager reciprocal relations $L_{ij} = L_{ji}$ (Groot & Mazur 1985, and see, for example, Qian *et al.* 2006; Eck *et al.* 2009). From (3.37), (3.33) and (3.35), we see that our choices of $\boldsymbol{\tau}$, \mathbf{q}_E and \mathbf{q}_C satisfy the linear relation (3.48) and also the reciprocal relations. Moreover, the entropy generation (3.45) is zero when the thermodynamic equilibrium conditions are satisfied within the system (i.e. thermodynamic forces are zero at equilibrium).

3.2.3. Galilean invariance

Another requirement that the entropy generation (3.45) should satisfy is that it be invariant under a Galilei transformation (Groot & Mazur 1985), since the notions of reversible and irreversible behaviour must be invariant under such a transformation. It can be seen that the entropy generation (3.45) satisfies this requirement automatically. Moreover, the model equations must be Galilean invariant as well, where, according to classical mechanics, the balance equations must be the same in the inertia frames. It can be observed that our system equations satisfy this requirement. It should be noted that, in another phase-field model (Abels, Garcke & Grun 2010), the volume-averaged velocity is employed, which leads to a non-objective scalar term appearing in the chemical potential equation. Therefore, a particular formulation for the convective terms is needed to keep the Galilean invariance of their model equations. In our model equations, on the other hand, the mass-averaged velocity is employed for the mixture; therefore no non-objective terms are involved. The system equations satisfy Galilean invariance automatically.

4. Phase-field model for quasi-incompressible fluid with thermocapillary effects

In this section, we develop a model of a binary Cahn–Hilliard fluid with thermocapillary effects in which both components are incompressible.

4.1. Derivation of the model

In order to study situations in which the density in each phase is uniform, it is convenient to adopt a thermodynamic formulation which does not employ the density as an independent variable, as in the model of quasi-incompressible flow considered by Lowengrub & Truskinovsky (1998). Following their work, we choose the pressure and temperature as independent variables, and work with the Gibbs free energy. In addition, for a binary incompressible fluid system, the free energy density can appear as the ‘per unit mass’ quantity or ‘per unit volume’ quantity. In most phase-field models for two-phase flows (e.g. Hohenberg & Halperin 1977; Liu & Shen 2002), the densities of the two components are assumed to be constant and equal, and the per unit mass and per unit volume specifications of the free energy density are equivalent. However, in the situation we study here, the densities of the two fluids of the mixture may not be matched and thus the per unit mass and per unit volume forms are not equivalent. As mentioned above, several models have been developed for binary incompressible fluids with different densities, in which the per unit volume form of the free energy density was employed by Boyer (2002), Ding *et al.* (2007), Shen & Yang (2010) and Abels *et al.* (2012) and the per unit mass form by Lowengrub & Truskinovsky (1998). Here, we concentrate on the Gibbs free energy density in the per unit mass form, and denote it by $\hat{g}(T, p, c, \nabla c)$. Again, similarly to the definition of the free energy (3.9) for binary compressible fluid, we introduce the gradient terms (gradient energy) into the Gibbs free energy of our model, which can then be given in the form

$$\hat{g}(T, p, c, \nabla c) = g(T, p, c) + g^{grad}(T, \nabla c), \quad g^{grad} = f^{grad} = \lambda_f(T) \frac{1}{2} |\nabla c|^2, \quad (4.1a,b)$$

where g is the classical part of the Gibbs free energy density and $\lambda_f(T)$ is a temperature-dependent coefficient and will lead to thermocapillary effects along

the interface (see §4.3 for details). For the classical part of the internal energy defined by (3.7), we have the following thermodynamic relation:

$$u(s, \rho, c) = g(T, p, c) + Ts - \frac{P}{\rho}. \tag{4.2}$$

Use of the thermodynamic relation (3.10) leads to

$$dg(T, p, c) = du(s, \rho, c) - d(sT) + d\left(\frac{P}{\rho}\right) = -sdT + \frac{1}{\rho}dp + \left.\frac{\partial u}{\partial c}\right|_{\rho,s} dc, \tag{4.3}$$

where we note the relations

$$\left.\frac{\partial g(T, p, c)}{\partial T}\right|_{p,c} = -s, \quad \left.\frac{\partial g(T, p, c)}{\partial p}\right|_{T,c} = \frac{1}{\rho} \quad \text{and} \quad \left.\frac{\partial g(T, p, c)}{\partial c}\right|_{T,p} = \left.\frac{\partial u}{\partial c}\right|_{\rho,s}. \tag{4.4a-c}$$

Here, as we notice that the variable density is independent of temperature and pressure (see (2.5)), the condition of incompressibility can then be written in the terms of the Gibbs free energy,

$$\frac{\partial^2 g(T, p, c)}{\partial^2 p} = 0, \tag{4.5}$$

where the second condition in (4.4) is used. Condition (4.5) implies that the Gibbs free energy is a linear function of pressure (e.g. Lowengrub & Truskinovsky 1998),

$$g(T, p, c) = g_0(T, c) + \frac{P}{\rho(c)}. \tag{4.6}$$

We then redefine the classical internal energy as a function of T , p and c ,

$$\tilde{u}(T, p, c) = u(s, \rho, c) = g(T, p, c) + Ts - \frac{P}{\rho(c)}, \tag{4.7}$$

where the relations (4.3) and (4.4) still hold. Similarly to the definition of the internal energy (3.7) and entropy (3.8) for the binary compressible fluid model, the specific internal energy \hat{u} and the specific entropy \hat{s} for binary incompressible fluids can be redefined in the form

$$\hat{u}(T, p, c, \nabla c) = \tilde{u}(T, p, c) + u^{grad}(\nabla c), \quad u^{grad} = \lambda_u \frac{1}{2} |\nabla c|^2, \tag{4.8}$$

$$\hat{s}(T, c, \nabla c) = \tilde{s}(T, c) + s^{grad}(\nabla c), \quad s^{grad} = \lambda_s \frac{1}{2} |\nabla c|^2, \tag{4.9}$$

where \tilde{u} and \tilde{s} are the classical parts of the specific internal energy and entropy associated with the Gibbs free energy, and λ_u and λ_s are constant. In addition to these classical contributions, we assume that the same thermodynamic relations that hold for the classical terms also hold for the total terms, such that

$$\hat{g} = \hat{u} - T\hat{s} + \frac{P}{\rho} = \hat{f} + \frac{P}{\rho}, \quad \left.\frac{\partial \hat{g}}{\partial T}\right|_{p,c,\nabla c} = -\hat{s}. \tag{4.10a,b}$$

Thus, from (4.1), (4.7)–(4.9), the relation for the coefficients (3.16) holds as well. The specifications of these three coefficients will be discussed in §4.2. It should be noted that λ_u and λ_s together with $\lambda_f(T)$ (in (4.1)) can be further used to relate the surface tension of the phase-field model to that of the sharp-interface model when our phase-field model reduces to its sharp-interface limit (see §5.4 for details).

Now we derive the system of equations for the quasi-incompressible phase-field model. We still use (3.1)–(3.5) to define the total properties, namely mass M , momentum \mathbf{P} , energy E , entropy S and mass constituent C in a material control

volume $V(t)$ of the domain Ω . We further assume that the corresponding general balance laws (3.17)–(3.21) that hold for the binary compressible fluid also hold for the quasi-incompressible fluid, which can then be written as

$$\frac{D\rho}{Dt} = -\rho(\nabla \cdot \mathbf{v}), \tag{4.11}$$

$$\rho \frac{D\mathbf{v}}{Dt} = \nabla \cdot \mathbf{m} - \rho g \hat{\mathbf{z}}, \tag{4.12}$$

$$\begin{aligned} \rho \frac{D\tilde{u}}{Dt} = & -\nabla \cdot \left(\rho \lambda_u \frac{Dc}{Dt} \nabla c \right) + \rho \lambda_u \Delta c \frac{Dc}{Dt} \\ & + (\mathbf{m} - \rho \lambda_u |\nabla c|^2 \mathbf{I} + \rho \lambda_u \mathbf{T}) : \nabla \mathbf{v} - \nabla \cdot \mathbf{q}_E - \nabla \cdot \mathbf{q}_E^{nc}, \end{aligned} \tag{4.13}$$

$$\begin{aligned} \rho \frac{D\tilde{s}}{Dt} = & -\nabla \cdot \left(\rho \lambda_s \frac{Dc}{Dt} \nabla c \right) + \rho \lambda_s \Delta c \frac{Dc}{Dt} \\ & - (\rho \lambda_s |\nabla c|^2 \mathbf{I} - \rho \lambda_s \mathbf{T}) : \nabla \mathbf{v} - \nabla \cdot \left(\frac{\mathbf{q}_E}{T} \right) - \nabla \cdot \mathbf{q}_S^{nc} + S_{gen}, \end{aligned} \tag{4.14}$$

$$\rho \frac{Dc}{Dt} = -\nabla \cdot \mathbf{q}_C, \tag{4.15}$$

where, as the pressure p is not defined in the traditional way, the general stress tensor \mathbf{m} is not defined explicitly.

It should be noted that, in contrast to the case of binary compressible fluid, the classical part of the internal energy \tilde{u} we defined here does not depend on the entropy \tilde{s} directly. However, as the derivations are carried out within the thermodynamic framework which is based on the entropy generation, a thermodynamic relation between the internal energy and the entropy is still needed. Having in mind the definition of the internal energy (4.7) and using the relations (4.3) and (4.4), we obtain the following relation between the classical part of the internal energy \tilde{u} , the Gibbs free energy g and the entropy \tilde{s} :

$$\rho \frac{D\tilde{u}}{Dt} = \rho \frac{\partial g_0}{\partial c} \frac{Dc}{Dt} + \rho T \frac{D\tilde{s}(T, c)}{Dt}. \tag{4.16}$$

Then similarly to the method used for the binary compressible fluid model, we use the unknowns, including \mathbf{m} , \mathbf{q}_E , \mathbf{q}_E^{nc} and \mathbf{q}_S^{nc} , to express the entropy generation in the form

$$\begin{aligned} S_{gen} = & \frac{1}{T} (\mathbf{m} - \rho \lambda_f(T) |\nabla c|^2 \mathbf{I} + \rho \lambda_f(T) \mathbf{T}) : \nabla \mathbf{v} \\ & + \nabla \cdot \frac{1}{T} \cdot \left(\rho \lambda_u \frac{Dc}{Dt} \nabla c + \mathbf{q}_E + \mathbf{q}_E^{nc} - \tilde{\mu}_C \mathbf{q}_C \right) \\ & - \nabla \cdot \left[\frac{1}{T} \left(\rho \lambda_f(T) \frac{Dc}{Dt} \nabla c + \mathbf{q}_E^{nc} - \tilde{\mu}_C \mathbf{q}_C - T \mathbf{q}_S^{nc} \right) \right] - \frac{1}{T} \mathbf{q}_C \cdot \nabla \tilde{\mu}_C, \end{aligned} \tag{4.17}$$

where we have used (4.11)–(4.16). Here, $\tilde{\mu}_C = \partial g_0(c) / \partial c - \lambda_f(T) \Delta c$ is a potential term. As the pressure is no longer defined by the thermodynamic formulae in this model, we now derive the pressure in an alternative way that was used by Lowengrub & Truskinovsky (1998), where the pressure was obtained from the non-dissipated part of

the general stress \mathbf{m} . Considering a dissipative process, we denote the general stress tensor by $\mathbf{m} = \mathbf{m}_0 + \boldsymbol{\tau}$, in which $\boldsymbol{\tau}$ is the deviatoric stress tensor with zero trace, and \mathbf{m}_0 is the unknown part to be defined later. We then denote $\mathbf{D}\mathbf{v} = \nabla\mathbf{v} - (\nabla \cdot \mathbf{v})\mathbf{I}/3$ as the deviatoric part of $\nabla\mathbf{v}$ ($\text{tr } \mathbf{D}\mathbf{v} = 0$). The entropy expression (4.17) can be rewritten as

$$\begin{aligned}
 S_{gen} = & \frac{1}{T} \left(\mathbf{m}_0 - \rho\lambda_f(T)|\nabla c|^2\mathbf{I} + \rho\lambda_f(T)\mathbf{T} \right) : \mathbf{D}\mathbf{v} + \frac{1}{T} \boldsymbol{\tau} : \nabla\mathbf{v} \\
 & + \nabla \frac{1}{T} \cdot \left\{ \rho\lambda_u \frac{Dc}{Dt} \nabla c + \mathbf{q}_E + \mathbf{q}_E^{nc} \right. \\
 & \left. - \left(\tilde{\mu}_C + \left(\frac{1}{3} \text{tr } \mathbf{m}_0 - \frac{2}{3} \rho\lambda_f(T)|\nabla c|^2 \right) \frac{1}{\rho^2} \frac{d\rho}{dc} \right) \mathbf{q}_C \right\} \\
 & - \nabla \cdot \left\{ \frac{1}{T} \left[\rho\lambda_f(T) \frac{Dc}{Dt} \nabla c + \mathbf{q}_E^{nc} \right. \right. \\
 & \left. \left. - \left(\tilde{\mu}_C + \left(\frac{1}{3} \text{tr } \mathbf{m}_0 - \frac{2}{3} \rho\lambda_f(T)|\nabla c|^2 \right) \frac{1}{\rho^2} \frac{d\rho}{dc} \right) \mathbf{q}_C - T\mathbf{q}_S^{nc} \right] \right\} \\
 & - \frac{1}{T} \mathbf{q}_C \cdot \nabla \left(\tilde{\mu}_C + \left(\frac{1}{3} \text{tr } \mathbf{m}_0 - \frac{2}{3} \rho\lambda_f(T)|\nabla c|^2 \right) \frac{1}{\rho^2} \frac{d\rho}{dc} \right), \tag{4.18}
 \end{aligned}$$

where we have used the mass balance (4.11) and the following identity:

$$\begin{aligned}
 (\mathbf{m}_0 - \rho\lambda_f(T)|\nabla c|^2\mathbf{I} + \rho\lambda_f(T)\mathbf{T}) : \frac{1}{3}(\nabla \cdot \mathbf{v})\mathbf{I} \\
 = \frac{1}{3}(\text{tr } \mathbf{m}_0 - \rho\lambda_f(T)\text{tr } |\nabla c|^2\mathbf{I} + \rho\lambda_f(T)\text{tr } \mathbf{T})(\nabla \cdot \mathbf{v}) \\
 = \left(\frac{1}{3} \text{tr } \mathbf{m}_0 - \frac{2}{3} \rho\lambda_f(T)|\nabla c|^2 \right) (\nabla \cdot \mathbf{v}). \tag{4.19}
 \end{aligned}$$

Now we assume that the first two terms on the right-hand side of (4.18) are non-dissipative and define the pressure p by

$$-p = \frac{1}{3} \text{tr } \mathbf{m} = \frac{1}{3} \text{tr}(\mathbf{m}_0 - \rho\lambda_f(T)|\nabla c|^2\mathbf{I} + \rho\lambda_f(T)\mathbf{T}) = \frac{1}{3} \text{tr } \mathbf{m}_0 - \frac{2}{3} \rho\lambda_f(T)|\nabla c|^2, \tag{4.20}$$

such that

$$-p\mathbf{I} = \mathbf{m}_0 - \rho\lambda_f(T)|\nabla c|^2\mathbf{I} + \rho\lambda_f(T)\mathbf{T}, \tag{4.21}$$

in which the way we use to define the pressure in (4.20) is analogous to the way that defines the kinematic pressure for the classical Navier–Stokes equations (Batchelor 2000). To ensure that our model is consistent with the second law of thermodynamics ($S_{gen} \geq 0$), we specify the unknown terms as follows:

$$\mathbf{q}_E = -k(c)\nabla T, \quad \mathbf{q}_E^{nc} = -\rho\lambda_u \frac{Dc}{Dt} + \mu_C \mathbf{q}_C, \tag{4.22}$$

$$\mathbf{q}_S^{nc} = -\rho\lambda_s \frac{Dc}{Dt} \nabla c, \quad \mathbf{m}_0 = -p\mathbf{I} + \rho\lambda_f(T)|\nabla c|^2\mathbf{I} - \rho\lambda_f(T)\mathbf{T}, \tag{4.23}$$

$$\mu_C = \frac{\partial g_0}{\partial c} - \frac{p}{\rho^2} \frac{d\rho}{dc} - \lambda_f(T)\Delta c, \quad \mathbf{q}_C = -m_C \nabla \mu_C, \tag{4.24}$$

$$\mathbf{T} = \nabla c \otimes \nabla c, \quad \boldsymbol{\tau} = \mu(c)(\nabla\mathbf{v} + \nabla\mathbf{v}^T) - \frac{2}{3}\mu(c)(\nabla \cdot \mathbf{v})\mathbf{I}. \tag{4.25}$$

Here, $\mathbf{m} = \mathbf{m}_0 + \boldsymbol{\tau}$. It should be noted that, comparing with the model developed by Lowengrub & Truskinovsky (1998), an extra term, $\rho\lambda_f(T)|\nabla c|^2\mathbf{I}$, appears in the stress tensor \mathbf{m}_0 (4.23). This term could be absorbed into the pressure for convenience (see Hua *et al.* 2011; Liu & Shen 2002 for examples). However, we still keep this term in order that the surface gradient of the surface tension in the sharp-interface limit can be recovered (see § 5.4 for details). This treatment is similar to that used by Guo *et al.* (2014*b*) and Garcke *et al.* (2014), where in Garcke *et al.* (2014) this term is also required to recover the surface gradient term in the asymptotic analysis. Apart from the momentum equation, the pressure appears in the chemical potential equation as well, which is different from the chemical potential (3.43) for the binary compressible fluid model. By substituting the above terms into (4.11)–(4.15), we obtain the system of equations for the phase-field model governing the quasi-incompressible fluid with thermocapillary effects,

$$\frac{D\rho}{Dt} = -\rho(\nabla \cdot \mathbf{v}), \tag{4.26}$$

$$\rho \frac{D\mathbf{v}}{Dt} = \nabla \cdot \mathbf{m} - \rho g \hat{\mathbf{z}}, \tag{4.27}$$

$$\begin{aligned} \rho \frac{D\tilde{u}}{Dt} &= \lambda_u \nabla \cdot (\rho \nabla c) \frac{Dc}{Dt} + (-p\mathbf{I} - \rho T \lambda_s |\nabla c|^2 \mathbf{I} + \rho T \lambda_s \boldsymbol{\tau} + \boldsymbol{\tau}) : \nabla \mathbf{v} \\ &\quad + \nabla \cdot (k(c) \nabla T + m_C \mu_C \nabla \mu_C), \end{aligned} \tag{4.28}$$

$$\begin{aligned} \rho \frac{D\tilde{s}}{Dt} &= \lambda_s \nabla \cdot (\rho \nabla c) \frac{Dc}{Dt} + \frac{1}{T} (-\rho T \lambda_s |\nabla c|^2 \mathbf{I} \\ &\quad + \rho T \lambda_s \boldsymbol{\tau} + \boldsymbol{\tau}) : \nabla \mathbf{v} + \frac{1}{T} \nabla \cdot (k(c) \nabla T), \end{aligned} \tag{4.29}$$

$$\rho \frac{Dc}{Dt} = m_C \Delta \mu_C, \tag{4.30}$$

$$\mu_C = \frac{\partial g_0}{\partial c} - \frac{p}{\rho^2} \frac{d\rho}{dc} - \lambda_f(T) \Delta c. \tag{4.31}$$

By multiplying (4.26), (4.27) and (4.29)–(4.31) by $p/\rho + \mathbf{v} \cdot \mathbf{v}/2 + u$, \mathbf{v} , T , μ_C and $\rho Dc/Dt$, and summing them up, we can obtain the first law of thermodynamics (3.19) that we used to derive the model. By substituting the terms, including \mathbf{m} , \mathbf{q}_E , \mathbf{q}_E^{nc} , \mathbf{q}_S^{nc} and \mathbf{q}_C , into the entropy generation (4.18), we obtain the second law of thermodynamics for our phase-field model,

$$S_{gen} = \frac{1}{T} \boldsymbol{\tau} : \nabla \mathbf{v} + k(c) \left| \frac{\nabla T}{T} \right|^2 + \frac{m_C}{T} |\nabla \mu_C|^2 \geq 0. \tag{4.32}$$

Similarly to the binary compressible model, the choices of the terms $\boldsymbol{\tau}$, \mathbf{q}_E and \mathbf{q}_C satisfy the linear relation (3.48) and the Onsager reciprocal relations (§ 3.2.2). Moreover, it can be observed that the entropy generation (4.32) and the system equations are Galilean invariant.

As mentioned above, several phase-field models have been developed for two-phase flows with thermocapillary effects. However, in most of these models, the classical energy balance equation,

$$\rho c_{hc} \frac{DT}{Dt} = \nabla \cdot (k \nabla T), \tag{4.33}$$

was incorporated directly into the phase-field model, where thermodynamic consistency can hardly be maintained. Compared with the classical energy balance equation (4.33), several extra terms appear in our energy balance equation (4.28), which guarantee thermodynamic consistency (see §4.2).

It should be noted that, if we define a new pressure as $\bar{p} = p - \rho\lambda_f(T)|\nabla c|^2$, and substitute it into the system (4.26)–(4.31), our model, in the isothermal case, reduces to the quasi-incompressible NSCH model developed by Lowengrub & Truskinovsky (1998).

By using the variable mass density (2.5), the mass balance equation (4.26) can be further rewritten as

$$\nabla \cdot \mathbf{v} = -\frac{1}{\rho} \frac{D\rho}{Dt} = \alpha\rho \frac{Dc}{Dt} = \alpha m_c \Delta\mu_c, \tag{4.34}$$

where we have used the Cahn–Hilliard equation (4.30) and let $\alpha = (\rho_2 - \rho_1)/\rho_2\rho_1$.

The initial conditions are given by

$$\mathbf{v}|_{t=0} = \mathbf{v}_0, \quad c|_{t=0} = c_0 \quad \text{and} \quad T|_{t=0} = T_0. \tag{4.35a-c}$$

For the velocity, the usual no-slip boundary conditions can be posed on $\partial\Omega$,

$$\mathbf{v} = \mathbf{v}_b. \tag{4.36}$$

For the phase field, it is normal to employ Neumann boundary conditions on $\partial\Omega$,

$$\nabla c \cdot \hat{\mathbf{n}} = h_c \quad \text{and} \quad \nabla\mu_c \cdot \hat{\mathbf{n}} = h_\mu. \tag{4.37a,b}$$

For the temperature, Dirichlet and Neumann boundary conditions can be posed on $\partial\Omega$,

$$T = T_b \quad \text{or} \quad \nabla T \cdot \hat{\mathbf{n}} = q_b, \tag{4.38a,b}$$

for the specified temperature and heat flux on the boundary $\partial\Omega$ respectively, and Robin boundary conditions can be posed as well.

4.2. Specifications of the model

We now specify the properties including the Gibbs free energy, entropy and internal energy for our phase-field model (4.26)–(4.31). In Anderson, McFadden & Wheeler (2000), a phase-field model for the solidification of a pure material that includes convection in the liquid phase was developed, in which the case of quasi-incompressibility (assuming that the density in each phase is uniform) was discussed. In their work, the Gibbs free energy was suggested in the form

$$\hat{g}(T, p, c, \nabla c) = g_0(T, c) + \frac{p}{\rho(c)} + \lambda_f(T) \frac{1}{2} |\nabla c|^2, \tag{4.39}$$

$$g_0(T, c) = (u_0 - c_{hc}T_0) \left(1 - \frac{T}{T_0}\right) - c_{hc}T \ln\left(\frac{T}{T_0}\right) + \gamma_f(T)h(c), \tag{4.40}$$

which we have adopted for the present work. Here, c_{hc} is the heat capacity, T_0 is the reference temperature, \tilde{u}_0 is the reference internal energy corresponding to T_0 and

$\gamma(T)$ is a temperature-dependent parameter that will be discussed later in this section. The free energy function $h(c)$ is a double-well potential and is given by

$$h(c) = \frac{c^2(c - 1)^2}{4}, \tag{4.41}$$

where the wells define the phases, and lead to an interfacial layer with large variations for c (e.g. Gurtin *et al.* 1996). It should be noted that the form for \hat{g} (4.39) is consistent with the incompressible condition (4.6), which is a linear function of pressure. Moreover, this form for \hat{g} is consistent with an internal energy \hat{u} , which is a linear function of temperature and leads to the classical heat equation in the bulk liquid (Wang *et al.* 1993; Anderson, McFadden & Wheeler 2001). The corresponding expressions for the entropy and internal energy are assumed in the form

$$\hat{s} = \tilde{s} + s^{nc} = \frac{1}{T_0} u_0 + c_{hc} \ln\left(\frac{T}{T_0}\right) + \gamma_s h(c) + \lambda_s \frac{1}{2} |\nabla c|^2, \tag{4.42}$$

$$\hat{u} = \tilde{u} + u^{nc} = \tilde{u}_0 + c_{hc}(T - T_0) + \gamma_u h(c) + \lambda_u \frac{1}{2} |\nabla c|^2, \tag{4.43}$$

where \tilde{u}_0 is the reference internal energy corresponding to T_0 .

We now specify those coefficients, including $\lambda_f(T)$, λ_s , λ_u , $\gamma_f(T)$, γ_s and γ_u , that are used to define the internal energy, entropy and free energy of the system (4.39)–(4.43). In the sharp-interface model for thermocapillary flow, the interface is usually represented as a surface of zero thickness with the surface tension as its physical property. An equation of state is required to relate the surface tension to the temperature, where, for the sake of simplicity, we only consider a linear relation in this study,

$$\sigma(T) = \sigma_0 - \sigma_T(T - T_0), \tag{4.44}$$

where σ_0 is the interfacial tension at the reference temperature T_0 , and σ_T is the rate of change of interfacial tension with temperature, defined as $\sigma_T = \partial\sigma(T)/\partial T$. In our phase-field model, however, the interface has finite thickness and the extra reactive stress (Ericksen’s stress) \mathbf{T} (4.25) appears in the Navier–Stokes equation to mimic the surface tension, where the coefficient of \mathbf{T} ,

$$\lambda_f(T) = \lambda_u - T\lambda_s, \tag{4.45}$$

is a linear function of temperature. We then try to relate $\sigma(T)$ and $\lambda(T)$ by introducing two parameters. The first parameter is ϵ with respect to the diffuse-interface thickness and the second one is η , a ratio parameter that relates the two surface tensions. As the interface thickness goes to zero, our phase-field model reduces to its sharp-interface limit, and the value of η can then be determined (see §5.4 for details). The corresponding coefficients can then be given as

$$\lambda_f(T) = \eta\epsilon\sigma(T) = \eta\epsilon\sigma_0 - \eta\epsilon\sigma_T(T - T_0), \quad \gamma_f(T) = \frac{\eta}{\epsilon}\sigma(T) = \frac{\eta}{\epsilon}\sigma_0 - \frac{\eta}{\epsilon}\sigma_T(T - T_0), \tag{4.46a,b}$$

$$\lambda_s = \eta\epsilon\sigma_T, \quad \gamma_s = \frac{\eta}{\epsilon}\sigma_T, \tag{4.47a,b}$$

$$\lambda_u = \eta\epsilon\sigma_0 + \eta\epsilon\sigma_T T_0, \quad \gamma_u = \frac{\eta}{\epsilon}\sigma_0 + \frac{\eta}{\epsilon}\sigma_T T_0. \tag{4.48a,b}$$

Here, the coefficients $\lambda_f(T)$, λ_s and λ_u for the gradient terms are of $O(\epsilon^2)$ of the coefficients $\gamma_f(T)$, γ_s and γ_u for the corresponding classical terms, which agrees with the definition of the Cahn–Hilliard free energy (e.g. Lowengrub & Truskinovsky 1998; Liu & Shen 2002). With the specifications above, the total energy E of our phase-field model can now be written as

$$E = \int_{V(t)} \left(\frac{1}{2} \rho |\mathbf{v}|^2 + \rho g z + \rho \tilde{u}_0 + \rho c_{hc}(T - T_0) + \rho \gamma_u h(c) + \rho \lambda_u \frac{1}{2} |\nabla c|^2 \right) dV. \tag{4.49}$$

4.3. Non-dimensionalization

With the help of the specification in (4.8), we non-dimensionalize the phase-field model (4.26)–(4.28), (4.30) and (4.31) as follows. We let L^* , V^* and T^* denote the characteristic scales of length, velocity and temperature. Then we introduce the dimensionless variables $\bar{\mathbf{x}} = \mathbf{x}/L^*$, $\bar{t} = V^*t/L^*$, and also $\bar{\epsilon} = \epsilon/L^*$, $\bar{\mathbf{v}} = \mathbf{v}/V^*$, $\bar{p} = p\rho_1\mu_c^*$, $\bar{\mu}_c = \mu_c/\mu_c^*$. For the variable density $\rho(c)$, viscosity $\mu(c)$ and thermal conductivity $k(c)$, (2.5) and (3.44), we let ρ_i , μ_i and k_i ($i = 1, 2$) denote the corresponding properties of the i th fluid, and introduce the dimensionless variables $\bar{\rho}_r = \rho(c)/\rho_1$, $\bar{\mu}_r = \mu(c)/\mu_1$ and $\bar{k}_r = k(c)/k_1$. Moreover, for the temperature field, we introduce a new dimensionless variable $\bar{T} = (T - T_0)/T^*$. The surface tension $\sigma(T)$ (4.44) is scaled by σ_0 such that $\bar{\sigma}(T) = \sigma(T)/\sigma_0$. Then σ_T is scaled by σ_0/T^* , such that $\bar{\sigma}_T = \sigma_T T^*/\sigma_0$. Omitting the bar notation, our phase-field model can now be rewritten as

$$\nabla \cdot \mathbf{v} = -\frac{1}{\rho_r} \frac{\partial \rho_r}{\partial c} \frac{Dc}{Dt}, \tag{4.50}$$

$$\begin{aligned} \rho_r \frac{D\mathbf{v}}{Dt} = & -\frac{1}{M} [\nabla p - Ca \nabla(\rho_r \sigma(T) |\nabla c|^2) + Ca \nabla \cdot (\rho_r \sigma(T) \mathbf{T})] \\ & + \frac{1}{Re} \nabla \cdot \left(\mu_r (\nabla \mathbf{v} + \nabla \mathbf{v}^T) - \frac{2}{3} \mu_r (\nabla \cdot \mathbf{v}) \mathbf{I} \right) - \frac{\rho_r}{Fr^2} \hat{\mathbf{z}}, \end{aligned} \tag{4.51}$$

$$\rho \frac{Dc}{Dt} = \frac{1}{Pe} \Delta \mu_c, \tag{4.52}$$

$$\mu_c = \frac{Ca}{\epsilon^2} \sigma(T) \frac{dh(c)}{dc} - \frac{p}{\rho_r^2} \frac{d\rho_r}{dc} - \frac{Ca}{\rho_r} \sigma(T) \Delta c, \tag{4.53}$$

$$\begin{aligned} \rho_r c_{hc} \frac{DT}{Dt} = & \frac{EcCa}{M} (1 + \sigma_T T_0) \nabla \cdot (\rho_r \nabla c) \frac{Dc}{Dt} \\ & + \frac{Ec}{M} \left(-p \mathbf{I} - Ca \rho_r T \sigma_T |\nabla c|^2 \mathbf{I} + Ca \rho_r T \sigma_T \mathbf{T} + \frac{1}{Re} \boldsymbol{\tau} \right) : \nabla \mathbf{v} \\ & + \nabla \cdot \left(\frac{1}{Ma} k_r \nabla T + \frac{Ec}{M Pe} \mu_c \nabla \mu_c \right), \end{aligned} \tag{4.54}$$

where $M = V^2/\mu_c$ is an analogue of the Mach number, $Ca = \eta \epsilon \sigma_0/\mu_c L$ is the capillary number, which measures the thickness of the interface, $Re = \mu_1/\rho_1 VL$ is the Reynolds number, $Fr = V^2/gL$ is the Froude number, $Pe = \rho LV/m_c \mu_c$ is the diffusional Peclet number, $Ec = V^2/c_{ch} T$ is the Eckert number, which characterizes energy dissipation, and $Ma = \rho c_{ch} VL/k_1$ is the Marangoni number. It should be noted that these non-dimensional system equations will be computed to study the effects of the Marangoni number through the example of thermocapillary migration of a drop. See § 6.5 for details.

5. Sharp-interface limits

Theoretically, there are usually two ways to validate the phase-field model. The first, as mentioned above, is to show thermodynamic consistency of the model. The second is to relate the phase-field model to its sharp-interface counterpart. Based on the assumption that a given sharp-interface formulation is the correct description of the physics under consideration, the phase-field model can be justified by simply showing that it is asymptotic to the classical sharp-interface description. In the isothermal case, some sharp-interface limit analyses have been carried out for the phase-field model of two-phase flow to show that the corresponding sharp-interface equations and jump conditions across the interface can be recovered from the phase-field model (e.g. Lowengrub & Truskinovsky 1998; Wang & Wang 2007; Abels *et al.* 2012). However, much less attention has been paid to the asymptotic analysis of the phase-field model for two-phase flows in the non-isothermal case, (e.g. thermocapillary flows, solidifications). Antanovskii (1995) presented a phase-field model to study the thermocapillary flow, and showed that the hydrostatic equilibrium condition for the case of a flat interface and the Laplace–Young condition for the case of a drop in equilibrium can be recovered from his phase-field model. Jasnow & Vinals (1996) extended model H to study thermocapillary flow, including the migration of a drop and spinodal decomposition of a binary fluid under a constant temperature gradient. In the corresponding sharp-interface limit, they showed that the additional stress term in the Navier–Stokes equation of their phase-field model is equivalent to the tangential and normal forces of the appropriate sharp-interface model. Anderson *et al.* (2000) developed a phase-field model of solidification with convection in the melt, in which the two phases are considered as viscous liquids. In the sharp-interface analysis (Anderson *et al.* 2001), they used the matched asymptotic expansions to show that the standard boundary conditions, including Young–Laplace and Stefan conditions, can be recovered from their phase-field model.

5.1. Pillbox argument

In this section, we apply a pillbox argument to our phase-field model (4.26)–(4.31). In contrast to the sharp-interface model, the interface of the phase-field model is diffusive with finite thickness $O(\epsilon)$. The phase variable (here the mass concentration c) is chosen to characterize the different phases, which take distinct values (here $c = 0, 1$) for the different phases, and change rapidly through the interfacial region. Within this interfacial region, we chose a contour line of c (here $c = 0.5$) to represent the dividing surface Γ for the following derivations (see Gibbs 1928; Everett 1972; Rowlinson & Widom 1982 for details of the dividing surface). Moreover, as the largest variations of the phase variable occur in the direction normal to the interface, the side faces of the pillbox need to be treated carefully. Figure 1 shows the pillbox-shaped control volume designed for our phase-field model, where the surface is divided into three parts, namely the top S_{top} , bottom S_{bot} and side S_{side} surfaces with their unit normal vectors \hat{n}_T , \hat{n}_B and \hat{n}_S respectively. The volume of the pillbox is $V = V_1 + V_2$, where V_i is the volume of a single component. The pillbox has a thickness of 2δ , where the top of the pillbox is above the dividing surface Γ at a height $\zeta = \delta$ and the bottom is below Γ at a height $\zeta = -\delta$. Here, ζ is a local coordinate normal to the interface Γ . In addition, the pillbox contains a portion of the diffuse interface with thickness $O(\epsilon)$, in which Γ stands for the dividing surface with its normal and tangent unit vectors \hat{n}_I and \hat{m}_I . The key limit in the pillbox argument is that $\epsilon \ll \delta \ll L$, where L is a length scale associated with the outer flow. In this limit, the

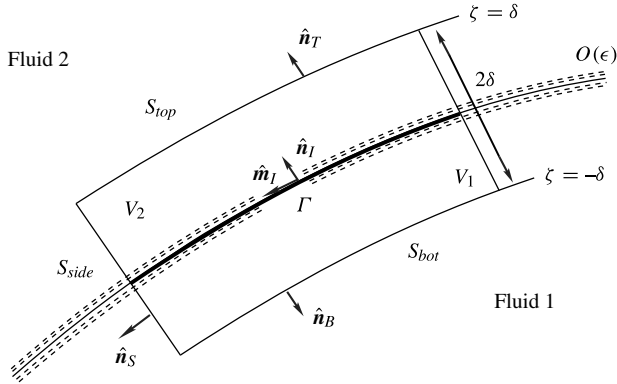


FIGURE 1. A schematic diagram showing a diffuse interface between two fluids intersecting with a pillbox-shaped control volume. Here, \hat{n}_T , \hat{n}_B and \hat{n}_S stand for the unit normal vector of the pillbox boundary on its top, bottom and side respectively. The dotted lines represent the diffuse interface with thickness $O(\epsilon)$. The thickness of the pillbox is 2δ . In the limit $\epsilon \ll \delta \ll L$, the interface thickness goes to zero, and the interface has constant density. Here, \hat{n}_I and \hat{m}_I stand for the unit normal and tangent vectors of the interface.

volume of the pillbox becomes negligible on the outer scales, but the variations in the concentration variable c that defines the interfacial region occur over a region fully contained within the pillbox. Also in this limit, the top (S_{top}) and bottom surfaces (S_{bot}) of the pillbox collapse onto the interface Γ , and have normal vectors with opposite directions,

$$S_{top} = S_{bot} = \Gamma, \quad \hat{n}_T = \hat{n}_I, \quad \hat{n}_B = -\hat{n}_I \quad \text{and} \quad \hat{n}_S = \hat{m}_I. \quad (5.1a-d)$$

Moreover, we assume that the dividing interface is moving with the velocity \mathbf{v}_I (Anderson & McFadden 1996; Anderson *et al.* 1998).

5.2. Governing equations in the sharp-interface limit

We first derive the system of equations in bulk regions away from the interfacial region. Here, we only concentrate on the equations of mass, momentum and energy balance. The system of (4.26)–(4.28) reduces to the classical equations appropriate for incompressible flows in bulk regions,

$$\nabla \cdot \mathbf{v} = 0, \quad (5.2)$$

$$\rho_i \frac{D\mathbf{v}}{Dt} = -\nabla p + \nabla \cdot (\mu_i (\nabla \mathbf{v} + \nabla \mathbf{v}^T)) - \rho_i g \hat{\mathbf{z}}, \quad (5.3)$$

$$\rho_i c_{hc} \frac{DT}{Dt} = \nabla \cdot (k_i \nabla T) + \mu_i (\nabla \mathbf{v} + \nabla \mathbf{v}^T) : \nabla \mathbf{v}, \quad (5.4)$$

where ρ_i , μ_i and k_i are the corresponding physical properties for the i th fluid. We now seek to derive the jump conditions for (5.2)–(5.4) at the interface from our phase-field model (4.26)–(4.31).

5.3. Jump condition for mass balance

In the limit $\epsilon \ll \delta \ll L$, we have the properties (Anderson & McFadden 1996; Anderson *et al.* 1998)

$$\int_V \frac{\partial \rho}{\partial t} dV \sim - \int_S \rho \mathbf{v}_I \cdot \hat{\mathbf{n}} dS, \tag{5.5}$$

$$\int_V \frac{\partial(\rho \mathbf{v})}{\partial t} dV \sim - \int_S \rho \mathbf{v} \otimes \mathbf{v}_I \cdot \hat{\mathbf{n}} dS. \tag{5.6}$$

On substituting (5.5) into the integral of equation (4.11) and using the divergence theorem we obtain

$$\int_S \rho(\mathbf{v} - \mathbf{v}_I) \cdot \hat{\mathbf{n}} dS = 0. \tag{5.7}$$

According to our pillbox argument, we break up the above surface integral into pieces for the top, bottom and side surfaces to obtain

$$\int_{S_{top}} \rho(\mathbf{v} - \mathbf{v}_I) \cdot \hat{\mathbf{n}}_T dS + \int_{S_{bot}} \rho(\mathbf{v} - \mathbf{v}_I) \cdot \hat{\mathbf{n}}_B dS + \oint_C \int_{-\delta}^{\delta} \rho(\mathbf{v} - \mathbf{v}_I) \cdot \hat{\mathbf{n}}_S d\zeta dl = 0. \tag{5.8}$$

Here, the surface integral of the side portion is further written in terms of a line integral on the surface and an integral in the normal direction $\hat{\mathbf{n}}_S$, where the line is a closed curve at the side of the control volume that parallel to the interface. For viscous fluid under normal operating conditions, it is an experimentally observed fact (like the no-slip boundary conditions at solid walls) that no slip takes place at the interface (Tryggvason, Scardovelli & Zaleski 2011). Therefore, in the limit $\epsilon \ll \delta \ll L$, we have

$$\mathbf{v} \cdot \hat{\mathbf{m}}_I \sim \mathbf{v}_I \cdot \hat{\mathbf{m}}_I. \tag{5.9}$$

This condition implies that the third term on the left in (5.8) is bounded and does not contribute to the integral. Equation (5.8) can be reduced to

$$\int_{\Gamma} [\rho(\mathbf{v} - \mathbf{v}_I)] \cdot \hat{\mathbf{n}}_I dS = 0, \tag{5.10}$$

where $[\chi] = \chi_2 - \chi_1$ refers to the jump of the quantity χ across the singular interface. Since the pillbox control volume V that contains a portion of the diffuse interface is arbitrary, the integrand in (5.10) must be zero. This then yields the mass balance jump condition at the interface in a two-phase fluid system,

$$[\rho(\mathbf{v} - \mathbf{v}_I)] \cdot \hat{\mathbf{n}}_I = 0. \tag{5.11}$$

Further, if we assume that there is no phase change (i.e. no flux) across the interface, (5.11) reduces to the jump condition that

$$[\mathbf{v}] \cdot \hat{\mathbf{n}}_I = 0. \tag{5.12}$$

5.4. *Jump condition for momentum balance*

By substituting (5.6) into the integral of momentum equation (4.27), we obtain

$$\int_S \left(\rho \mathbf{v} \otimes (\mathbf{v} - \mathbf{v}_I) + p\mathbf{I} - \eta \epsilon \sigma(T) \rho |\nabla c|^2 \mathbf{I} + \eta \epsilon \sigma(T) \rho \mathbf{T} - \mu(\nabla \mathbf{v} + \nabla \mathbf{v}^T) + \frac{2}{3} \mu(\nabla \cdot \mathbf{v}) \mathbf{I} \right) \cdot \hat{\mathbf{n}} dS = 0, \tag{5.13}$$

where we have used the mass balance equation (4.26), such that

$$\rho \frac{D\mathbf{v}}{Dt} = \rho \frac{D\mathbf{v}}{Dt} + \left(\frac{D\rho}{Dt} + \rho(\nabla \cdot \mathbf{v}) \right) \mathbf{v} = \frac{\partial(\rho \mathbf{v})}{\partial t} + \nabla \cdot (\rho \mathbf{v} \otimes \mathbf{v}). \tag{5.14}$$

Moreover, in the limit $\epsilon \ll \delta \ll L$, we assume that the gravitational term $\rho g \hat{\mathbf{z}}$ is bounded and thus does not contribute to the volume integral. We then break up the above surface integral into pieces for the top, bottom and sides of the pillbox to obtain

$$\begin{aligned} & \int_{S_{top}} \left(\rho \mathbf{v} \otimes (\mathbf{v} - \mathbf{v}_I) + p\mathbf{I} - \eta \epsilon \sigma(T) \rho |\nabla c|^2 \mathbf{I} + \eta \epsilon \sigma(T) \rho \mathbf{T} - \mu(\nabla \mathbf{v} + \nabla \mathbf{v}^T) + \frac{2}{3} \mu(\nabla \cdot \mathbf{v}) \mathbf{I} \right) \cdot \hat{\mathbf{n}}_T dS \\ & + \int_{S_{bot}} \left(\rho \mathbf{v} \otimes (\mathbf{v} - \mathbf{v}_I) + p\mathbf{I} - \eta \epsilon \sigma(T) \rho |\nabla c|^2 \mathbf{I} + \eta \epsilon \sigma(T) \rho \mathbf{T} - \mu(\nabla \mathbf{v} + \nabla \mathbf{v}^T) + \frac{2}{3} \mu(\nabla \cdot \mathbf{v}) \mathbf{I} \right) \cdot \hat{\mathbf{n}}_B dS \\ & + \oint_C \int_{-\delta}^{\delta} \left(\rho \mathbf{v} \otimes (\mathbf{v} - \mathbf{v}_I) + p\mathbf{I} - \eta \epsilon \sigma(T) \rho |\nabla c|^2 \mathbf{I} + \eta \epsilon \sigma(T) \rho \mathbf{T} - \mu(\nabla \mathbf{v} + \nabla \mathbf{v}^T) + \frac{2}{3} \mu(\nabla \cdot \mathbf{v}) \mathbf{I} \right) \cdot \hat{\mathbf{n}}_S d\zeta dl = 0. \end{aligned} \tag{5.15}$$

We assume that the most rapid variations in the phase field take place across the interfacial region with the direction normal to the interface Γ . In the limit $\epsilon \ll \delta \ll L$, local to the interface we have (Anderson & McFadden 1996; Lowengrub & Truskinovsky 1998)

$$\nabla \sim \frac{\partial}{\partial \zeta} \hat{\mathbf{n}}_I, \quad \nabla c \sim \frac{\partial c}{\partial \zeta} \hat{\mathbf{n}}_I \quad \text{and} \quad \Delta c \sim \frac{\partial^2 c}{\partial \zeta^2}, \tag{5.16a-c}$$

such that

$$\mathbf{T} = \nabla c \otimes \nabla c \sim \frac{\partial c}{\partial \zeta} \hat{\mathbf{n}}_I \frac{\partial c}{\partial \zeta} \hat{\mathbf{n}}_I, \quad \mathbf{T} \cdot \hat{\mathbf{n}}_I \sim \frac{\partial c}{\partial \zeta} \frac{\partial c}{\partial \zeta} \hat{\mathbf{n}}_I \quad \text{and} \quad \mathbf{T} \cdot \hat{\mathbf{m}}_I \sim 0. \tag{5.17a-c}$$

Condition (5.9) implies that the fluid velocity term $\rho \mathbf{v} \otimes (\mathbf{v} - \mathbf{v}_I) \cdot \hat{\mathbf{n}}_S$ is bounded and does not contribute to the integral over the side surface of the pillbox. The terms $-\mu(\nabla \mathbf{v} + \nabla \mathbf{v}^T) \cdot \hat{\mathbf{n}}_S$ are bounded and do not contribute to the side integral. We argue that the term $2/3\mu(\nabla \cdot \mathbf{v})$ is bounded across the interfacial region and thus does not

contribute to the side integral. The pressure p is bounded and does not contribute to the side integral. Further, the non-classical stress term \mathbf{T} does not contribute to the integral over the top and bottom surfaces. Equation (5.15) reduces to

$$\int_{\Gamma} ([\rho \mathbf{v}(\mathbf{v} - \mathbf{v}_I)] \cdot \hat{\mathbf{n}}_I + [p\mathbf{I}] \cdot \hat{\mathbf{n}}_I + [-\mu(\nabla \mathbf{v} + \nabla \mathbf{v}^T)] \cdot \hat{\mathbf{n}}_I) dS - \oint_C \int_{-\delta}^{\delta} \eta \epsilon \sigma(T) \rho \left(\frac{\partial c}{\partial \zeta} \right)^2 \hat{\mathbf{m}}_I d\zeta dl = 0, \tag{5.18}$$

where the condition (5.1) is used. Here, for our pillbox argument to make sense, we require that within the pillbox the temperature is continuous and the variations are small over a small distance (of the order of the pillbox thickness δ). In the limit $\epsilon \ll \delta \ll L$, the temperature T is approximately uniform along the direction normal to the interface. It should be noted that a similar assumption for the temperature was also suggested by Jasnow & Vinals (1996), where a surface tension term with thermocapillary effects was identified from a phase-field model in its sharp-interface limit. Denoting the surface tension by

$$\tilde{\sigma}(T) = \eta \sigma(T) \lim_{\epsilon \rightarrow 0} \int_{-\delta}^{\delta} \left(\epsilon \rho \left(\frac{\partial c}{\partial \zeta} \right)^2 \right) d\zeta, \tag{5.19}$$

and substituting into (5.18), we obtain

$$\int_{\Gamma} ([\rho \mathbf{v}(\mathbf{v} - \mathbf{v}_I)] \cdot \hat{\mathbf{n}}_I + [p\mathbf{I}] \cdot \hat{\mathbf{n}}_I + [-\mu(\nabla \mathbf{v} + \nabla \mathbf{v}^T)] \cdot \hat{\mathbf{n}}_I) dS - \oint_C \tilde{\sigma} \hat{\mathbf{m}}_I dl = 0, \tag{5.20}$$

where, in the limit $\epsilon \ll \delta \ll L$, we assume that the tangential unit vector $\hat{\mathbf{m}}_I$ is independent of ζ and thus can be taken out of the line integral. Use of the surface divergence theorem (Weatherburn 1939) leads to

$$\oint_C \tilde{\sigma} \hat{\mathbf{m}}_I dl = \int_{\Gamma} \nabla_s \tilde{\sigma} dS - \int_{\Gamma} (\nabla_s \cdot \hat{\mathbf{n}}_I) \tilde{\sigma} \hat{\mathbf{n}}_I dS. \tag{5.21}$$

By substituting (5.21) into (5.20), we obtain

$$[\rho \mathbf{v}(\mathbf{v} - \mathbf{v}_I)] \cdot \hat{\mathbf{n}}_I + [p\mathbf{I}] \cdot \hat{\mathbf{n}}_I + [-\mu(\nabla \mathbf{v} + \nabla \mathbf{v}^T)] \cdot \hat{\mathbf{n}}_I = \nabla_s \tilde{\sigma} + \kappa \tilde{\sigma} \hat{\mathbf{n}}_I. \tag{5.22}$$

Here, ∇_s is the surface gradient and $\kappa = -\nabla_s \cdot \hat{\mathbf{n}}_I$ is the mean curvature of the surface (e.g. Weatherburn 1939). The first term on the right is the tangential thermocapillary (Marangoni) force that accounts for the non-uniform surface tension, while the second is the normal surface tension force. Again, if we assume that there is no phase change (i.e. no flux) across the interface, (5.22) reduces to the jump condition that

$$[p\mathbf{I}] \cdot \hat{\mathbf{n}}_I + [-\mu(\nabla \mathbf{v} + \nabla \mathbf{v}^T)] \cdot \hat{\mathbf{n}}_I = \nabla_s \tilde{\sigma} + \kappa \tilde{\sigma} \hat{\mathbf{n}}_I, \tag{5.23}$$

which is the classical momentum balance jump condition at the interface for two-phase incompressible fluid with thermocapillary effects.

It should be noted that we can relate the surface tension of our phase-field model $\tilde{\sigma}(T)$ (identified in (5.19)) to that of the sharp-interface model $\sigma(T)$ (defined in (4.44))

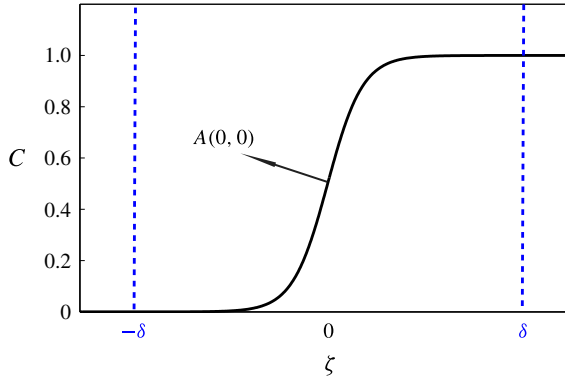


FIGURE 2. (Colour online) The stationary solution c_0 (solid line) for the phase field. Here, A is a point on the dividing surface Γ , and δ and $-\delta$ are the positions of the top and bottom surfaces of the pillbox (dotted lines).

by letting

$$\tilde{\sigma}(T) = \eta \sigma(T) \int_{-\delta}^{+\delta} \epsilon \rho(c) \left(\frac{dc}{d\zeta} \right)^2 d\zeta = \sigma(T). \tag{5.24}$$

The value of the ratio parameter η can then be determined through the following equation:

$$\eta = \frac{1}{\int_{-\delta}^{+\delta} \epsilon \rho(c) \left(\frac{dc}{d\zeta} \right)^2 d\zeta}. \tag{5.25}$$

It has been argued by Chella & Vinals (1996) that in the limit of a gently curved interface, and when the motion of the interface is slow, the phase variable c can be approximated by its 1D stationary solution c_0 along the direction normal to the interface. For simplicity, we now assume that the local coordinate ζ coincides with the y direction, and the position of the dividing surface is $y_0 = 0$. In the 1D case, we have the following stationary solution c_0 near the interfacial region:

$$c_0(y) = \frac{1}{2} + \frac{1}{2} \tanh\left(\frac{y}{2\sqrt{2}\epsilon}\right), \quad \text{for } y \in [-\delta, \delta], \tag{5.26}$$

which is shown in figure 2. Here, $y = \delta$ and $y = -\delta$ are the positions of the top and bottom surfaces of the pillbox separately. In the limit $\epsilon \ll \delta \ll L$, we note the conditions

$$c = \begin{cases} 0, & \text{for } y = \delta, \\ 1, & \text{for } y = -\delta. \end{cases} \tag{5.27}$$

By substituting (5.26) and the variable density (2.5) into (5.25) we obtain

$$\eta = \frac{2\sqrt{2}(\rho_2 - \rho_1)^3}{\rho_1 \rho_2 \left[\rho_2^2 - \rho_1^2 - 2\rho_1 \rho_2 \ln\left(\frac{\rho_2}{\rho_1}\right) \right]}, \tag{5.28}$$

where the condition (5.27) is used. It should be noted that for the density matched case ($\rho_1 = \rho_2$), (5.25) leads to a simpler expression for η , which is

$$\eta = 6\sqrt{2}. \tag{5.29}$$

This agrees with the result obtained by Rowlinson & Widom (1982), Yue *et al.* (2004) and Aland (2012). In § 6, we will compute some examples by using our phase-field model for quasi-incompressible fluids (4.26)–(4.31).

5.5. Jump condition for energy balance

To derive the jump condition for the energy balance at the interface, we first substitute the terms E , \mathbf{m} , \mathbf{q}_E and \mathbf{q}_E^{nc} (3.3), (4.22), (4.23) and (4.25) into the energy balance equation (3.19). In the integral form, we obtain

$$\begin{aligned} & \int_S \left(\rho \hat{u}(\mathbf{v} - \mathbf{v}_I) + \rho \frac{1}{2} |\mathbf{v}|^2 (\mathbf{v} - \mathbf{v}_I) + \left(p \mathbf{I} - \eta \epsilon \sigma(T) \rho |\nabla c|^2 \mathbf{I} + \eta \epsilon \sigma(T) \rho \mathbf{T} \right. \right. \\ & \quad \left. \left. - \mu (\nabla \mathbf{v} + \nabla \mathbf{v}^T) + \frac{2}{3} \mu (\nabla \cdot \mathbf{v}) \mathbf{I} \right) \cdot \mathbf{v} - \lambda_u \left(\rho \nabla c \frac{Dc}{Dt} \right) \right. \\ & \quad \left. - k \nabla T - m_C \mu_C \nabla \mu_C \right) \cdot \hat{\mathbf{n}}_I dS = 0, \end{aligned} \tag{5.30}$$

where we have used the identities

$$\rho \frac{D\hat{u}}{Dt} = \frac{\partial(\rho \hat{u})}{\partial t} + \nabla \cdot (\rho \hat{u} \mathbf{v}), \tag{5.31}$$

$$\rho \frac{D}{Dt} \frac{1}{2} |\mathbf{v}|^2 = \frac{\partial}{\partial t} \left(\rho \frac{1}{2} |\mathbf{v}|^2 \right) + \nabla \cdot \left(\rho \frac{1}{2} |\mathbf{v}|^2 \mathbf{v} \right), \tag{5.32}$$

and the following properties which are similar to (5.5) and (5.6):

$$\int_V \frac{\partial(\rho \hat{u})}{\partial t} dV \sim - \int_S \rho \hat{u} \mathbf{v}_I \cdot \hat{\mathbf{n}} dS, \tag{5.33}$$

$$\int_V \frac{\partial}{\partial t} \left(\rho \frac{1}{2} |\mathbf{v}|^2 \right) dV \sim - \int_S \rho \frac{1}{2} |\mathbf{v}|^2 \mathbf{v}_I \cdot \hat{\mathbf{n}} dS. \tag{5.34}$$

We then break up the above integral (5.30) into pieces for the top, bottom and sides of the pillbox to obtain

$$\begin{aligned} & \int_{S_{top}} \left(\rho \hat{u}(\mathbf{v} - \mathbf{v}_I) + \rho \frac{1}{2} |\mathbf{v}|^2 (\mathbf{v} - \mathbf{v}_I) + \left(p \mathbf{I} - \eta \epsilon \sigma(T) \rho |\nabla c|^2 \mathbf{I} + \eta \epsilon \sigma(T) \rho \mathbf{T} \right. \right. \\ & \quad \left. \left. - \mu (\nabla \mathbf{v} + \nabla \mathbf{v}^T) + \frac{2}{3} \mu (\nabla \cdot \mathbf{v}) \mathbf{I} \right) \cdot \mathbf{v} - \lambda_u \left(\rho \nabla c \frac{Dc}{Dt} \right) - k \nabla T - m_C \mu_C \nabla \mu_C \right) \cdot \hat{\mathbf{n}}_T dS \\ & + \int_{S_{bot}} \left(\rho \hat{u}(\mathbf{v} - \mathbf{v}_I) + \rho \frac{1}{2} |\mathbf{v}|^2 (\mathbf{v} - \mathbf{v}_I) + \left(p \mathbf{I} - \eta \epsilon \sigma(T) \rho |\nabla c|^2 \mathbf{I} + \eta \epsilon \sigma(T) \rho \mathbf{T} \right. \right. \\ & \quad \left. \left. - \mu (\nabla \mathbf{v} + \nabla \mathbf{v}^T) + \frac{2}{3} \mu (\nabla \cdot \mathbf{v}) \mathbf{I} \right) \cdot \mathbf{v} - \lambda_u \left(\rho \nabla c \frac{Dc}{Dt} \right) - k \nabla T - m_C \mu_C \nabla \mu_C \right) \cdot \hat{\mathbf{n}}_B dS \end{aligned}$$

$$\begin{aligned}
 & + \oint_C \int_{-\delta}^{\delta} \left(\rho \hat{u}(\mathbf{v} - \mathbf{v}_I) + \rho \frac{1}{2} |\mathbf{v}|^2 (\mathbf{v} - \mathbf{v}_I) + \left(p \mathbf{I} - \eta \epsilon \sigma(T) \rho |\nabla c|^2 \mathbf{I} + \eta \epsilon \sigma(T) \rho \mathbf{T} \right. \right. \\
 & - \mu (\nabla \mathbf{v} + \nabla \mathbf{v}^T) + \frac{2}{3} \mu (\nabla \cdot \mathbf{v}) \mathbf{I} \cdot \mathbf{v} - \lambda_u \left(\rho \nabla c \frac{Dc}{Dt} \right) - k \nabla T \\
 & \left. \left. - m_C \mu_C \nabla \mu_C \right) \cdot \hat{\mathbf{n}}_s d\zeta dl = 0, \tag{5.35}
 \end{aligned}$$

where we assume that the heat capacity c_{hc} is a constant. In the limit $\epsilon \ll \delta \ll L$, the non-classical terms of the internal energy \hat{u} (4.43), \mathbf{T} , $\lambda_u(\rho \nabla c(Dc/Dt))$ and $m_C \mu_C \nabla \mu_C$, do not contribute to the top and the bottom surface integrals. The non-classical term $m_C \mu_C \nabla \mu_C$ and the energy term $k \nabla T$ are bounded in the tangential direction and do not contribute to the side integral. Equation (5.35) then reduces to

$$\begin{aligned}
 & \int_{\Gamma} \left([\rho c_{hc} T(\mathbf{v} - \mathbf{v}_I)] + \left[\rho \frac{1}{2} |\mathbf{v}|^2 (\mathbf{v} - \mathbf{v}_I) \right] + [p \mathbf{I} \cdot \mathbf{v}] - [\mu (\nabla \mathbf{v} + \nabla \mathbf{v}^T) \cdot \mathbf{v}] \right. \\
 & \left. - [k \nabla T] \right) \cdot \hat{\mathbf{n}}_I dS - \oint_C \left(\int_{-\delta}^{\delta} \eta \epsilon \sigma(T) \rho \left(\frac{dc}{d\zeta} \right)^2 d\zeta \right) \mathbf{v}_I \cdot \hat{\mathbf{m}}_I dl = 0, \tag{5.36}
 \end{aligned}$$

where in the last term of (5.36), we argue that the interface velocity \mathbf{v}_I is independent of the local coordinate ζ and thus can be taken out of the integral in the normal direction. By using (5.19) and the surface divergence theorem, we obtain

$$\begin{aligned}
 [k \nabla T] \cdot \hat{\mathbf{n}}_I &= ([\rho c_{hc} T(\mathbf{v} - \mathbf{v}_I)] + [\rho \frac{1}{2} |\mathbf{v}|^2 (\mathbf{v} - \mathbf{v}_I)] + [p \mathbf{I} \cdot \mathbf{v}] \\
 & - [\mu (\nabla \mathbf{v} + \nabla \mathbf{v}^T) \cdot \mathbf{v}]) \cdot \hat{\mathbf{n}}_I - \nabla_s \cdot (\tilde{\sigma} \mathbf{v}_I) - \kappa \tilde{\sigma} \hat{\mathbf{n}}_I \cdot \mathbf{v}_I, \tag{5.37}
 \end{aligned}$$

where the energy spent by the interface deformation and the effects of the interface curvature are taken into account in our jump condition for the energy balance at the interface. Equation (5.37) agrees with the result obtained by Andrea (2011), where the energy balance condition at the interface is derived by using a pillbox for the sharp-interface model. Again if we assume that there is no phase change across the interface, (5.37) then reduces to

$$[k \nabla T] \cdot \hat{\mathbf{n}}_I = ([p \mathbf{I} \cdot \mathbf{v}] - [\mu (\nabla \mathbf{v} + \nabla \mathbf{v}^T) \cdot \mathbf{v}]) \cdot \hat{\mathbf{n}}_I - \nabla_s \cdot (\tilde{\sigma} \mathbf{v}_I) - \kappa \tilde{\sigma} \hat{\mathbf{n}}_I \cdot \mathbf{v}_I. \tag{5.38}$$

If we further ignore the energy spent by the interface deformation and the effects of interface curvature, we can obtain the classical jump condition for the energy equation,

$$[k \nabla T] \cdot \hat{\mathbf{n}}_I = 0, \tag{5.39}$$

which is widely used for the computations of the sharp-interface model (e.g. Tavener & Cliffe 2002).

6. Computational methods and results

In this section, we investigate our phase-field model numerically through three examples. One is the thermocapillary convection in a microchannel with two-layer superimposed fluid, and the second (third) one is the thermocapillary migration of a drop with zero (finite respectively) Marangoni number. All examples will be computed by using continuous finite element methods. The numerical results of the first and second examples will be compared with the existing analytical solutions and numerical results.

6.1. Simplified model and the weak form

For the sake of simplicity, we assume that the densities of the two fluids are matched. The system (4.26)–(4.31) can then be simplified in the form

$$\nabla \cdot \mathbf{v} = 0, \tag{6.1}$$

$$\frac{D\mathbf{v}}{Dt} = -\nabla p + \nabla[\lambda_f(T)|\nabla c|^2] - \nabla \cdot [\lambda_f(T)(\nabla c \otimes \nabla c)] + \nabla \cdot (\mu \nabla \mathbf{v}), \tag{6.2}$$

$$\begin{aligned} \frac{D\hat{u}}{Dt} &= \lambda_u \nabla \cdot \left(\nabla c \frac{Dc}{Dt} \right) + (-p\mathbf{I} + \lambda_f(T)|\nabla c|^2\mathbf{I} - \lambda_f(T)(\nabla c \otimes \nabla c) \\ &\quad + \mu \nabla \mathbf{v}) : \nabla \mathbf{v} + \nabla \cdot (k\nabla T + m_C \mu_C \nabla \mu_C), \end{aligned} \tag{6.3}$$

$$\frac{Dc}{Dt} = m_C \Delta \mu_C, \tag{6.4}$$

$$\mu_C = \gamma_f(T) \frac{dh(c)}{dc} - \lambda_f(T) \Delta c, \tag{6.5}$$

where the variable thermal conductivity (3.44) is employed. Here, we employed the energy balance equation (3.19) instead of (4.28). The reason is that in the weak formulation of (4.28), the second-order derivative is involved, implying that more reductive C^1 finite elements are needed for the conformity. However, in the weak formulation of (6.3) ((6.8) below) we find that only first-order derivatives of c are involved, so that the C^0 finite element method may be used for our computations. The benefits of using C^0 elements are obvious, in that the method can have more choices of elements and many existing codes can be incorporated to reduce various complications. It should be noted that (6.1)–(6.3) of the system will be computed for the example of thermocapillary convection, (6.1)–(6.5) will be computed for the example of thermocapillary migration with zero Marangoni number, and the non-dimensional system (4.50)–(4.54) will be computed for the example of thermocapillary migration with finite Marangoni number. For simplicity, we only present the numerical scheme for the dimensional system (6.1)–(6.5). The numerical method for the non-dimensional system (4.50)–(4.54) can be obtained correspondingly. By multiplying the system (6.1)–(6.5) by the test functions q , \mathbf{u} , χ , ϕ and ψ respectively and using integration by parts, the weak form can be derived straightforwardly (where \mathbf{v} , p , \hat{u} , c , μ and the test functions \mathbf{u} , q , χ , ϕ and ψ are in appropriate spaces),

$$\int_{\Omega} (\nabla \cdot \mathbf{v} q) dx = 0, \tag{6.6}$$

$$\begin{aligned} \int_{\Omega} (\mathbf{v}_t \cdot \mathbf{u} + (\mathbf{v} \cdot \nabla) \mathbf{v} \cdot \mathbf{u} - p \nabla \cdot \mathbf{u} + \lambda_f(T)(\nabla c \cdot \nabla c) \nabla \cdot \mathbf{u} \\ - \lambda_f(T)(\nabla c \otimes \nabla c) : \nabla \mathbf{u} + \mu \nabla \mathbf{v} : \nabla \mathbf{u}) dx = 0, \end{aligned} \tag{6.7}$$

$$\begin{aligned} \int_{\Omega} \left(\hat{u}_t \chi + (\mathbf{v} \cdot \nabla) \hat{u} \chi + \lambda_u \frac{Dc}{Dt} \nabla c \cdot \nabla \chi - \lambda_f(T)(\nabla c \cdot \nabla c)(\nabla \cdot \mathbf{v}) \chi \right. \\ \left. - \mu \nabla \mathbf{v} : \nabla \mathbf{v} \chi + \lambda_f(T)(\nabla c \otimes \nabla c) : \nabla \mathbf{v} \chi + p \mathbf{I} : \nabla \mathbf{v} \chi \right. \\ \left. + k \nabla T \cdot \nabla \chi + m_C \mu_C \nabla \mu_C \cdot \nabla \chi \right) dx = 0, \end{aligned} \tag{6.8}$$

$$\int_{\Omega} (c_t \phi + (\mathbf{v} \cdot \nabla) c \phi + m_C \nabla \mu_C \cdot \nabla \phi) dx = 0, \tag{6.9}$$

$$\int_{\Omega} \left(\mu_C \psi - \gamma_f(T) \frac{dh(c)}{dc} \psi - \nabla \lambda_f(T) \cdot \nabla c \psi - \lambda_f(T) \nabla c \cdot \nabla \psi \right) dx = 0. \tag{6.10}$$

6.2. Temporal schemes and implementation issues

The solution of the weak form (6.6)–(6.10) is approximated by a finite difference scheme in time and a conformal C^0 finite element method in space. To ensure the stability of our numerical method, we adopt the fully implicit backward Euler scheme to compute the problem.

We let $\Delta t > 0$ represent a time step size, and $(\mathbf{v}_h^n, p_h^n, \hat{u}_h^n, c_h^n, \mu c_h^n)$ (in a finite dimensional space given by a finite element discretization of the computational domain Ω) is an approximation of $(\mathbf{v}, p, \hat{u}, c, \mu)$ at time $t^n = n\Delta t$, where $\mathbf{v}_h^n = \mathbf{v}(n\Delta t)$, $p_h^n = p(n\Delta t)$, $\hat{u}_h^n = \hat{u}(n\Delta t)$, $c_h^n = c(n\Delta t)$ and $\mu c_h^n = \mu c(n\Delta t)$. Then the approximation at time t^{n+1} is denoted as $(\mathbf{v}_h^{n+1}, p_h^{n+1}, \hat{u}_h^{n+1}, c_h^{n+1}, \mu c_h^{n+1})$ and computed by the following finite element scheme:

$$\int_{\Omega} (\nabla \cdot \mathbf{v}_h^{n+1} q + \delta p_h^{n+1} q) dx = 0, \tag{6.11}$$

$$\int_{\Omega} (\mathbf{v}_i^{n+1} \cdot \mathbf{u} + (\mathbf{v}_h^{n+1} \cdot \nabla) \mathbf{v}_h^{n+1} \cdot \mathbf{u} - p_h^{n+1} \nabla \cdot \mathbf{u} + \lambda_f(T_h^{n+1})(\nabla c_h^{n+1} \cdot \nabla c_h^{n+1}) \nabla \cdot \mathbf{u} - \lambda_f(T_h^{n+1})(\nabla c_h^{n+1} \otimes \nabla c_h^{n+1}) : \nabla \mathbf{u} + \mu \nabla \mathbf{v}_h^{n+1} : \nabla \mathbf{u}) dx = 0, \tag{6.12}$$

$$\int_{\Omega} (\hat{u}_i^{n+1} \chi + (\mathbf{v}_h^{n+1} \cdot \nabla) \hat{u}_h^{n+1} \chi + \lambda_u(c_i^{n+1} + (\mathbf{v}_h^{n+1} \cdot \nabla) c_h^{n+1}) \nabla c_h^{n+1} \cdot \nabla \chi - \lambda_f(T_h^{n+1})(\nabla c_h^{n+1} \cdot \nabla c_h^{n+1})(\nabla \cdot \mathbf{v}_h^{n+1}) \chi + \lambda_f(T_h^{n+1})(\nabla c_h^{n+1} \otimes \nabla c_h^{n+1}) : \nabla \mathbf{v}_h^{n+1} \chi - \mu \nabla \mathbf{v}_h^{n+1} : \nabla \mathbf{v}_h^{n+1} \chi + k \nabla T_h^{n+1} \cdot \nabla \chi + m_c \mu c_h^{n+1} \nabla \mu c_h^{n+1} \cdot \nabla \chi) dx = 0, \tag{6.13}$$

$$\int_{\Omega} (c_i^{n+1} \phi + (\mathbf{v}_h^{n+1} \cdot \nabla) c_h^{n+1} \phi + m_c \nabla \mu c_h^{n+1} \cdot \nabla \phi) dx = 0, \tag{6.14}$$

$$\int_{\Omega} (\mu c_h^{n+1} \psi - \gamma_f(T_h^{n+1}) h'(c_h^{n+1}) \psi - \nabla \lambda_f(T_h^{n+1}) \cdot \nabla c_h^{n+1} \psi - \lambda_f(T_h^{n+1}) \nabla c_h^{n+1} \cdot \nabla \psi) dx = 0, \tag{6.15}$$

where $\mathbf{v}_i^{n+1} = (\mathbf{v}_h^{n+1} - \mathbf{v}_h^n) / \Delta t$, $\hat{u}_i^{n+1} = (\hat{u}_h^{n+1} - \hat{u}_h^n) / \Delta t$ and $c_i^{n+1} = (c_h^{n+1} - c_h^n) / \Delta t$. It should be noted that the divergence-free equation needs to be treated carefully in incompressible flow computations. Here, we rewrite (6.11) in the penalty formulation, where δ is a relatively small parameter and is set to be $\delta = 10^{-6}$ for all the computations. It should be noted that for every time step, T^{n+1} can be obtained by using (4.43), such that

$$c_{hc} T_h^{n+1} = \hat{u}_h^{n+1} - \gamma_u h(c_h^{n+1}) - \lambda_u \frac{1}{2} \nabla c_h^{n+1} \cdot \nabla c_h^{n+1}. \tag{6.16}$$

Since the scheme is nonlinearly implicit we need to perform the linearization and then solve a linear system iteratively at each time step. We follow the numerical methods designed by Hua *et al.* (2011), where the linear system is symmetric and does not depend on time. Therefore, we only need to perform the Cholesky factorization for the symmetric linear system at the initial time step. After the initial time we do not need to factorize the linear system again since the coefficient matrix is independent of time.

For a phase-field model, it is sufficient to finely resolve only the interfacial region, and a fixed grid meshing represents a waste of computational resources. Therefore, an efficient adapting mesh that resolves the thin interfacial region is desirable. For the examples of thermocapillary convection, we design a mesh that has relatively high-resolution grids near the flat interface. For the example of thermocapillary migration, since the interface moves as the drop rises, an adaptive mesh is designed, in which there is a smaller frame that moves with the drop. Within the frame, the resolution

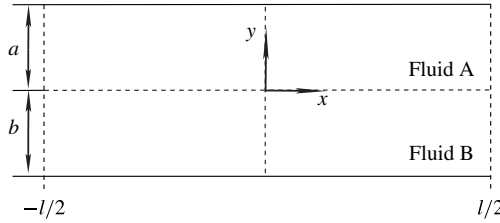


FIGURE 3. Schematic diagram showing two immiscible fluids in a microchannel. The temperatures of the lower and upper plates are $T^b(x, -b) = T_h + T_0 \cos(kx)$ and $T^a(x, a) = T_c$ respectively, where $T_h > T_c > T_0$ and $k = 2\pi/l$ is the wavenumber, and a and b are the heights of the fluids A and B respectively.

of grids is much higher than those outside the moving frame, so that the moving interface of the drop can be resolved purposely. Here, only the meshes for the example of thermocapillary migration are shown.

6.3. Thermocapillary convection in a two-layer fluid system

We now investigate the thermocapillary convection in a heated microchannel with two-layer superimposed fluids with a planar interface (Pendse & Esmaeeli 2010). We consider two-layer fluids (figure 3), where the heights of fluid A (upper) and fluid B (lower) are a and b respectively, and the fluids are of infinite extension in the horizontal direction. The physical properties of the fluids are their densities, viscosities and heat conductivities. The temperature variations in the present study are considered to be small enough so that the thermophysical properties of each fluid are assumed to remain constant, with the exception of surface tension. The temperatures of the lower and upper plates are

$$T^b(x, -b) = T_h + T_0 \cos(\omega x) \quad \text{and} \quad T^a(x, a) = T_c \tag{6.17a,b}$$

respectively, where $T_h > T_c > T_0 > 0$, and $\omega = 2\pi/l$ is a wavenumber with l being the channel length. The above temperature boundary conditions establish a temperature field that is periodic in the horizontal direction with a period of l . Therefore, it is sufficient to only focus on the solution in one period, i.e. $-l/2 < x < l/2$. In the limit of zero Marangoni number and small Reynolds number, it is possible to ignore the convective transport of momentum and energy. In addition, we assume that the interface is to remain flat. By solving the simplified sharp-interface governing equations with the corresponding jump boundary conditions at the interface, Pendse & Esmaeeli (2010) obtained the analytical solutions for the temperature field $\bar{T}(x, y)$ and stream function $\bar{\psi}(x, y)$, where for the upper fluid

$$\bar{T}^A(x, y) = \frac{(T_c - T_h)y + \tilde{k}T_c b + T_h a}{a + \tilde{k}b} + T_0 f(\alpha, \beta, \tilde{k}) \sinh(\alpha - \omega y) \cos(\omega x), \tag{6.18}$$

$$\begin{aligned} \bar{\psi}^A(x, y) = \frac{U_{max}}{\omega} \frac{1}{\sinh^2(\alpha) - \alpha^2} & \left\{ \omega y \sinh^2(\alpha) \cosh(\omega y) \right. \\ & \left. - \frac{1}{2} [2\alpha^2 + \omega y (\sinh(2\alpha) - 2\alpha)] \sinh(\omega y) \right\} \sin(\omega x), \end{aligned} \tag{6.19}$$

and for the lower fluid

$$\bar{T}^B(x, y) = \frac{\tilde{k}(T_c - T_h)y + \tilde{k}T_cb + T_ha}{a + \tilde{k}b} + T_0f(\alpha, \beta, \tilde{k}) [\sinh(\alpha) \cosh(\omega y) - \tilde{k} \sinh(\omega y) \cosh(\alpha)] \cos(\omega x), \tag{6.20}$$

$$\bar{\psi}^B(x, y) = \frac{U_{max}}{\omega} \frac{1}{\sinh^2(\beta) - \beta^2} \left\{ \omega y \sinh^2(\beta) \cosh(\omega y) - \frac{1}{2} [2\beta^2 - \omega y (\sinh(2\beta) - 2\beta)] \sinh(\omega y) \right\} \sin(\omega x). \tag{6.21}$$

In the above equations the unknowns are defined by $\tilde{k} = k_A/k_B$, $\alpha = a\omega$, $\beta = b\omega$, $f(\alpha, \beta, \tilde{k}) = 1/(\tilde{k} \sinh(\beta) \cosh \alpha + \sinh(\alpha) \cosh \beta)$, $g(\alpha, \beta, \tilde{k}) = \sinh(\alpha)f(\alpha, \beta, \tilde{k})$ and

$$U_{max} = - \left(\frac{T_0\sigma_T}{\mu_B} \right) g(\alpha, \beta, \tilde{k}) h(\alpha, \beta, \tilde{\mu}), \tag{6.22}$$

$$h(\alpha, \beta, \tilde{\mu}) = \frac{(\sinh^2(\alpha) - \alpha^2)(\sinh^2(\beta) - \beta^2)}{\tilde{k}(\sinh^2(\beta) - \beta^2)(\sinh(2\alpha) - 2\alpha) + (\sinh^2(\alpha) - \alpha^2)(\sinh(2\beta) - 2\beta)}. \tag{6.23}$$

Based on their work, the simulations for our phase-field model are carried out in a 2D domain $[-l/2, l/2] \times [-b, a]$ with $l = 1.6 \times 10^{-4}$ and $a = b = 4 \times 10^{-5}$. As the interface between the two fluids is assumed to be flat and rigid, the initial conditions for the phase variable only depend on y , and can be given in the form

$$c(y) = \frac{1}{2} + \frac{1}{2} \tanh\left(\frac{y}{2\sqrt{2}\epsilon}\right), \quad \text{for } y \in (-b, a). \tag{6.24}$$

The periodic boundary conditions are applied on the left and right sides of the domain. On the top and bottom walls, the no-slip boundary conditions are imposed such that

$$v = 0, \quad \text{for } y = a, -b. \tag{6.25}$$

Equations (6.17a,b) are used as the boundary conditions for temperature with $T_h = 20$, $T_c = 10$ and $T_0 = 4$. We let the ratio parameter $\eta = 6\sqrt{2}$ (5.29). Moreover, the fluid properties are shown in table 1. To show the influences of the thermal conductivity ratio on the stream-function and temperature fields, the simulations are carried out for two cases with different values of \tilde{k} , where $\tilde{k} = 0.1$ for case 1 and $\tilde{k} = 0.5$ for case 2. Here, the variable thermal conductivity $k(c)$ (3.44) is employed, where we fix $k_B (= 0.2)$, and change the value of k_A for the two cases. The contours of the temperature fields and stream functions for two cases at $\epsilon = 0.002$ are shown in figures 4 and 5 respectively. It can be seen that our numerical results are in good agreement with the analytical solutions. In order to show that our phase-field model approaches the sharp-interface model as the thickness of the diffuse interface goes to zero, the computations are carried out by using five different values of ϵ ($= 0.02, 0.01, 0.005, 0.002, 0.001$). The L^2 norms of the relative differences between the numerical results and analytical solutions are shown in table 2. We can observe that as the value of ϵ decreases, the L^2 norm of the relative differences decreases for both the temperature field and the stream function. We also note that there are slight

$$\mu_A = \mu_B = 0.2 \qquad k_B = 0.2 \quad \sigma_0 = 2.5 \times 10^{-1}$$

$$\tilde{k} = k_A/k_B \text{ (thermal conductivity ratio)} \quad \sigma_T = -5 \times 10^{-3} \text{ (at } T_{ref} = T_c)$$

TABLE 1. The physical properties of two fluids for the example of thermocapillary convection (A and B stand for fluids A and B separately).

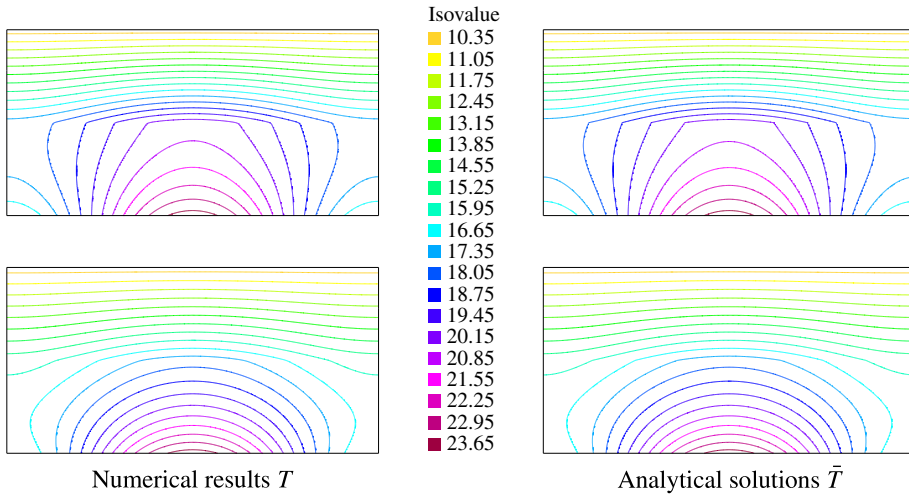


FIGURE 4. (Colour online) Isotherms of the numerical results and analytical solutions for the example of thermocapillary convection in a two-layer fluid system with different thermal diffusivity ratios $\tilde{k} = 0.1$ and $\tilde{k} = 0.5$.

differences between our numerical results and the analytical predictions. The reason is twofold. First, and most importantly, the thickness of the interface of our model is finite, and the thermal diffusivity changes across it. Second, the viscous heating term is considered in our energy balance equation (6.3). As can be observed from the isotherms in figure 4, the cosine-like boundary condition for temperature leads to non-uniform distributions of the temperature along the interface. This results in a shear force along the interface that is from the centre to both sides of the domain. The fluids are set in motion by this shear force and move from the middle towards both sides of the domain. These are then replaced by the fluid flowing downwards (upward) from the top (bottom) boundary. Also, as the domain is periodic in the horizontal direction, the velocities of fluids that move towards both sides decrease and the fluids are forced to move upward (downward) to the top (bottom) of the domain. This mechanism results in the formation of the circulation patterns that can be observed in the stream-function fields (figure 5), where the fluid flow consists of four counter-rotating circulations that divide the domain into four parts. Moreover, in the context of the thermal conductivity ratio, we find that the decrease of \tilde{k} leads to a more non-uniform distribution of temperature along the interface, and thus strengthens the thermocapillary convection. This result agrees with the recent result obtained by Liu *et al.* (2014), where the same thermocapillary convection in a two-layer fluid system was investigated numerically by using a lattice Boltzmann phase-field method.

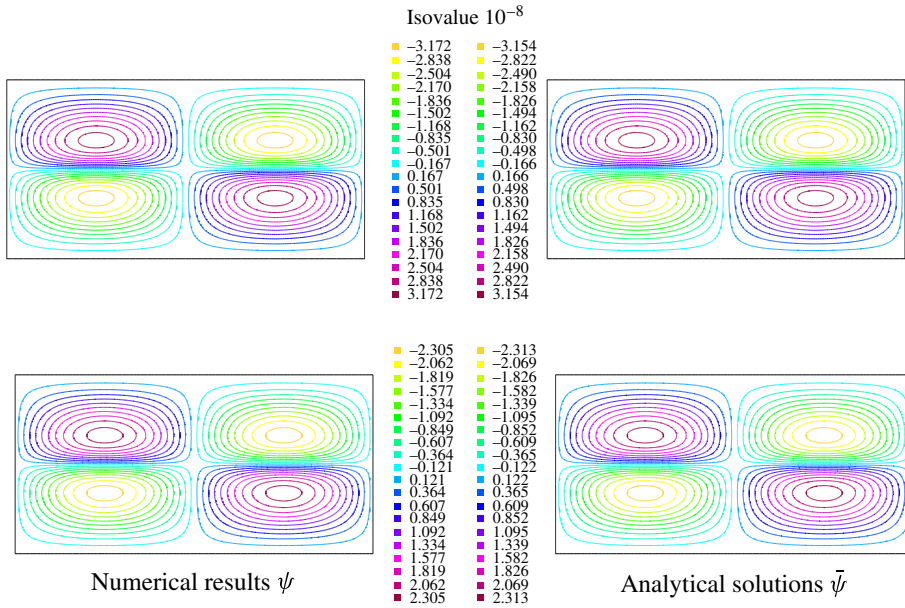


FIGURE 5. (Colour online) Streamlines of the numerical results and analytical solutions for the example of thermocapillary convection in a two-layer fluid system with different thermal diffusivity ratios $\tilde{k} = 0.1$ and $\tilde{k} = 0.5$. Positive (negative) values of the stream function indicate the clockwise (the counterclockwise) circulation.

6.4. *Thermocapillary migration in the limit of zero Marangoni number*

The thermocapillary migration of a drop was first examined experimentally by Young *et al.* (1959), who derived an analytical expression for the terminal velocity (also known as the YGB velocity) of the drop in an infinite domain. In this study, both the Marangoni and Reynolds numbers are assumed to be infinitely small, such that the convective transport of momentum and energy is negligible. Instead, the terminal velocity of the drop is derived in an infinite domain with constant temperature gradient fields, and can be given in the form

$$V_{YGB} = \frac{2U}{(2 + \tilde{k})(2 + 3\tilde{\mu})}, \tag{6.26}$$

where $U = -\sigma_T G_T R / \mu_B$ is chosen as the velocity scale, R is the radius of the drop, G_T stands for the constant temperature gradient, $\tilde{k} = k_A / k_B$ is the thermal conductivity ratio and $\tilde{\mu} = \mu_A / \mu_B$ is the viscosity ratio between the two fluids. In our simulation, we consider a 2D domain Ω of size $[0, 7.5R] \times [0, 15R]$ where a planar 2D circular drop of fluid A with radius $R = 0.1$ is placed inside the medium of fluid B, with the centre of the drop located at the centre of the box $(x_c, y_c) = (3.75R, 7.5R)$. We set the initial condition for the phase field as

$$c(x, y) = \frac{1}{2} \tanh\left(\frac{R - [(x - x_c)^2 + (y - y_c)^2]^{1/2}}{2\sqrt{2}\epsilon}\right) + \frac{1}{2}. \tag{6.27}$$

In figure 6 we present the initial condition (6.27) for the whole domain (left-hand side), and for fixed $x = 3.75R$ (right-hand side), where it can be observed that the

		$\epsilon = 0.02$	$\epsilon = 0.01$	$\epsilon = 0.005$	$\epsilon = 0.002$	$\epsilon = 0.001$
$k = 0.1$	$\frac{\ T - \bar{T}\ _{L^2}}{\ \bar{T}\ _{L^2}}$	5.445×10^{-3}	2.503×10^{-3}	1.189×10^{-3}	4.551×10^{-4}	2.200×10^{-4}
	$\frac{\ \psi - \bar{\psi}\ _{L^2}}{\ \bar{\psi}\ _{L^2}}$	4.309×10^{-2}	2.668×10^{-2}	1.614×10^{-2}	6.94×10^{-3}	6.44×10^{-3}
$k = 0.5$	$\frac{\ T - \bar{T}\ _{L^2}}{\ \bar{T}\ _{L^2}}$	1.585×10^{-3}	5.748×10^{-4}	2.098×10^{-4}	5.167×10^{-5}	1.815×10^{-5}
	$\frac{\ \psi - \bar{\psi}\ _{L^2}}{\ \bar{\psi}\ _{L^2}}$	6.796×10^{-2}	2.208×10^{-2}	8.682×10^{-3}	3.688×10^{-3}	7.318×10^{-4}

TABLE 2. The L^2 norm of the relative differences between the numerical results and the analytical solutions for § 6.3.

$$\sigma_0 = 5 \times 10^{-2}, \quad \sigma_T = 1.25 \times 10^{-3} \text{ (at } T_{ref} = T_b), \quad \mu_A = \mu_B = 0.2, \quad m_C = 0.1\epsilon.$$

TABLE 3. The physical properties of two fluids for the example of thermocapillary migration (A and B stand for the fluids A and B separately).

area with $c = 1$ represents the drop (fluid A) and the area with $c = 0$ represents the medium (fluid B), between which the value of c varies rapidly, resulting in a diffuse interface with finite thickness. Within this transition layer, the dotted contour line is at the level $c = 0.5$ representing the dividing surface Γ . No-slip boundary conditions are imposed on the top and bottom walls, and periodic boundary conditions are imposed in the horizontal direction. A linear temperature field is imposed in the y direction,

$$T(x, y) = T_b + \frac{T_t - T_b}{15R}y = T_b + G_T y, \tag{6.28}$$

with $T_b = 10$ on the bottom wall and $T_t = 25$ on the top wall, resulting in a constant temperature gradient, $G_T = 10$. Again, we let the ratio parameter $\eta = 6\sqrt{2}$ (5.29). Moreover, the fluid properties are shown in table 3. Using these values, the theoretical terminal velocity of a spherical drop can be given as

$$V_{YGB} = 8.333 \times 10^{-4}. \tag{6.29}$$

Numerically, we use the following equation to calculate the rise velocity v_r of the drop for our phase-field model:

$$v_r = \frac{\int_{\Omega} c \mathbf{v} \cdot \hat{\mathbf{j}} dV}{\int_{\Omega} c dV}, \tag{6.30}$$

where $\hat{\mathbf{j}}$ is the component of the unit vector in the y direction.

Figure 7 shows the temporal evolution of the drop velocity normalized by V_{YGB} between two different interface capturing methods, the phase-field method and level-set method (Herrmann *et al.* 2008). Similarly to the previous example in § 6.3,

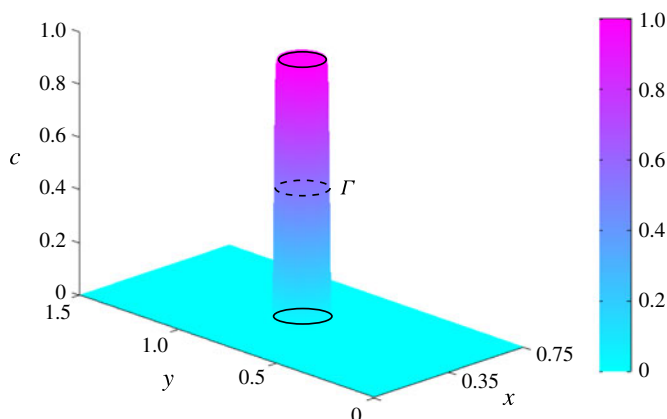


FIGURE 6. (Colour online) Initial condition of the phase variable c for the example of the thermocapillary migration of a drop. The dotted line stands for the dividing surface.

we compute our model by using two different interfacial thicknesses corresponding to $\epsilon = 0.002$ and 0.001 . Both the phase-field method and the level-set method seem to converge to a value of $v_r/V_{YGB} = 0.8$, roughly 20% different from the theoretical prediction. The reason for this discrepancy is twofold. First, and most importantly, the theoretical rise velocity is for an axisymmetric sphere, whereas our simulations are carried out for a planar 2D drop. Second, the simulations include small blockage effects from the finite computational domain size as well as minute deformations of the drop, whereas the theoretical formula assumes an infinite domain and a non-deformable drop. As the thickness of the diffuse interface decreases, our results seem to converge to the that obtained by the level-set method (Herrmann *et al.* 2008). For the case $\epsilon = 0.001$, we present the streamlines together with the moving interface at $t = 1$ and $t = 50$ in figure 8, where we observe that the streamlines for both cases exhibit similar patterns, with two asymmetric recirculations around the drop. Figure 8 shows the meshes together with the drop interface at $t = 1$ and $t = 50$. Here, the size of the smaller frame is set to be $[3R \times 3R]$, in which we take the shortest edge of the grids inside the frame as $15R/1000 = \epsilon$, so that at least 7–9 grid cells (corresponding to the definition of the interfacial thickness) are located across the interface to ensure accuracy of our computations. In addition, the moving velocity of the frame is set to be equal to the drop rising velocity $v_{frame} = v_r$, such that, through this relative long-term behaviour, the rising drop is always kept inside the smaller moving frame.

6.5. Thermocapillary migration with finite Marangoni number

We now compute the example of the thermocapillary motion of a drop with finite Marangoni number. Due to the finite Marangoni number, the energy equation (6.3) is coupled with the momentum equation (6.2). This is expected to result in a reduction of the tangential temperature gradients at the drop interface due to the interfacial flow driven by the Marangoni stress, which in turn will also be reduced. In this simulation, we consider a 2D domain Ω of size $[0, 10R] \times [0, 15R]$, where a planar 2D circular drop of fluid A with radius $R = 0.5$ is placed inside the medium of fluid B, with the centre of the drop located at the centre of the box $(x_c, y_c) = (0, 1.5R)$. At $t = 0$, (6.27) is employed as the initial condition for the phase variable, and a linear temperature

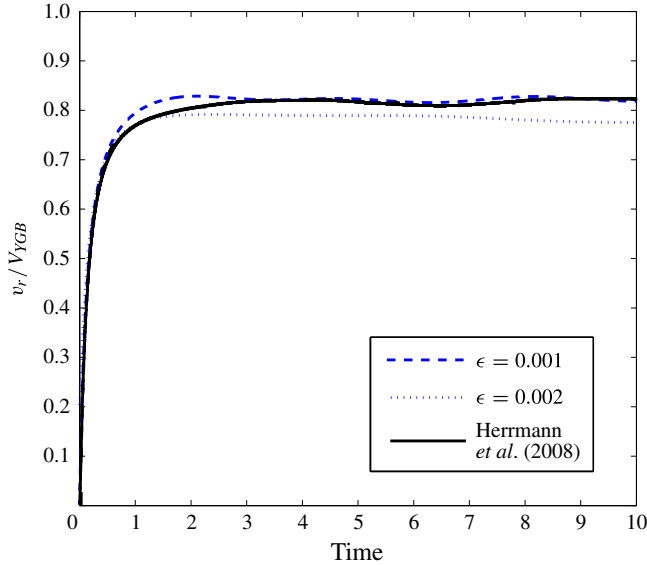


FIGURE 7. (Colour online) The time evolution of the normalized migration velocity of a drop. The dashed lines are our numerical results for a 2D planar drop (v_r), while the solid line represents the numerical results by using the level-set method.

distribution from $T_b = 0$ at the bottom to $T_t = 1$ at the top is imposed for the bulk liquid, and we assume that the drop has the same initial linear temperature distribution as the bulk liquid. Again, no-slip boundary conditions are imposed on the top and bottom boundaries, and periodic boundary conditions are imposed in the horizontal direction. The two fluids are assumed to have the same densities and viscosities. We set the thermal conductivity $k_1 = 0.1$ for the drop and $k_2 = 1$ for the bulk fluid. In this section, the non-dimensionalized system (4.50)–(4.54) is computed, where we set the non-dimensional parameters as $\epsilon = 0.002$, $Re = 10$, $M = 1$, $Pe = 100/\epsilon$, $Ca = 1$, $Ec = 1$. Five different values of the Marangoni number are employed for the computations, namely $Ma = 50, 100, 500, 1000, 1500$.

Figure 9 shows the velocity of the drop versus time for the five cases. As the time processes, the rise velocity reduces in all five cases, and we can observe that an increase in Ma leads to a decrease in the rise velocity, which is consistent with the simulations by Herrmann *et al.* (2008), Yin *et al.* (2008) and Zhao *et al.* (2010).

Figure 10 shows snapshots of the isotherms at four different times for the corresponding three cases, where the dependence of the migration velocity on the Marangoni number can be easily explained. Obviously, the enhanced convective transport of momentum and heat with increase of the Marangoni number results in more disturbances of the temperature field. Inside the drop, as we increase the Marangoni number, larger variations can be observed, leading to a substantial reduction in the surface temperature gradient and the corresponding rise velocities.

7. Conclusion and future work

In this paper, we present a thermodynamically consistent phase-field model for two-phase flows with thermocapillary effects, which allows a binary incompressible fluid (quasi-incompressible fluid) to have different physical properties for each

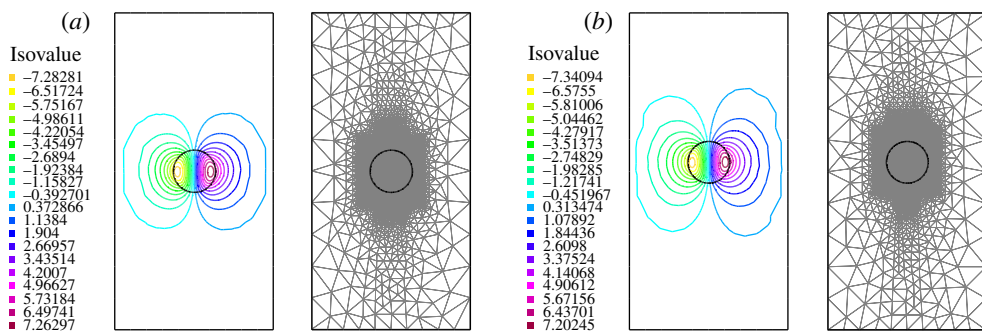


FIGURE 8. (Colour online) The drop interface (black) and the streamlines (grey-scale lines, left), and the meshes (grey lines, right) at (a) $t = 1$ and (b) $t = 50$. Positive values of the stream function indicate the clockwise circulation and negative values of the stream function indicate the counterclockwise circulation.

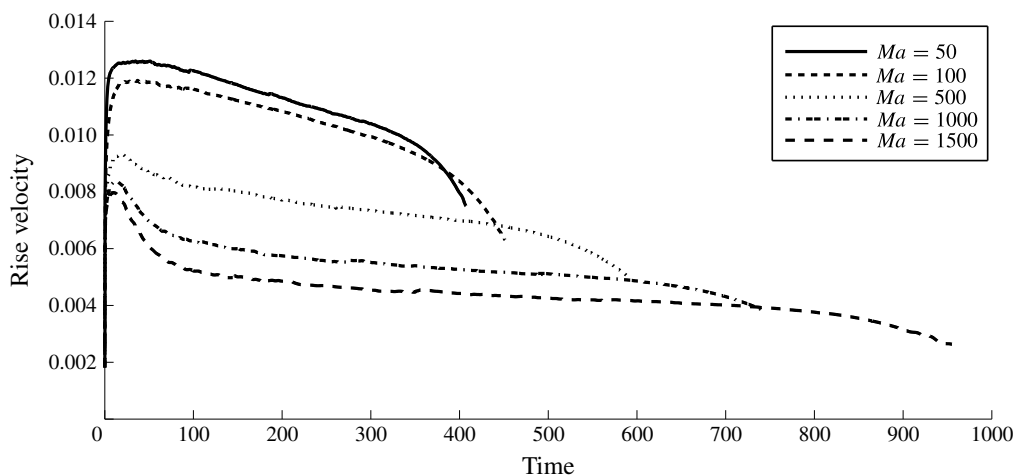


FIGURE 9. The time evolution of the rise velocity of a drop with different finite Marangoni numbers.

component, including densities, viscosities and thermal conductivities. To the best of our knowledge, such a phase-field model is new. We chose the mass concentration as the phase variable, and the corresponding variable density and mass-averaged velocity lead to a quasi-incompressible formulation for the binary incompressible fluid. As the thermocapillary effects are produced by the non-homogenous distribution of a temperature-dependent (linear) surface tension, we introduce the square-gradient (Cahn–Hilliard) term into the internal energy and entropy of our phase-field model, so that the interfacial free energy that is associated with the surface tension in our model can be linearly dependent on the temperature. Our model equations, including the mass balance equation, Navier–Stokes equation with extra stress term, advective Cahn–Hilliard equation, energy balance equation and entropy balance equation, are derived within a thermodynamic frame based on entropy generation. Compared with the classical energy balance equation employed by other phase-field models, the non-classical terms associated with the square-gradient term appear in our energy

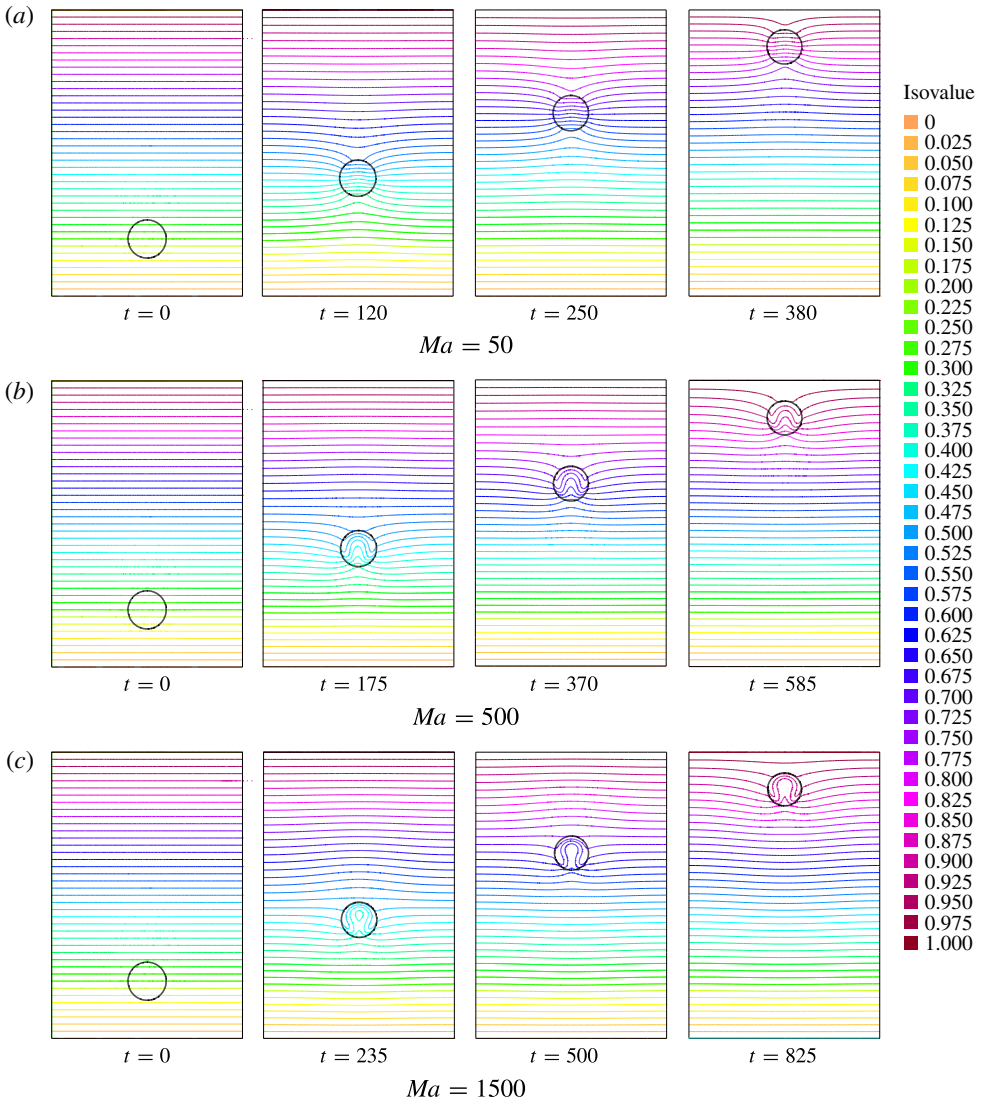


FIGURE 10. (Colour online) Snapshots of the drop interface (black) and isotherms (grey-scale lines) for different times and different values of Ma as indicated.

balance equation (4.28) to account for the energy spent by the variations of the phase field. In addition, we verify the first and second thermodynamic laws from the system of equations to show that thermodynamic consistency is maintained in our model. Moreover, we have also verified that our system equations satisfy the important modelling properties, namely the Onsager reciprocal relations and Galilean invariance.

In the sharp-interface analysis, we show that the system of equations and jump conditions at the interface for the classical sharp-interface model are recovered from our model, which reveals the underlying physical mechanisms of the phase-field model, and provides a validation of our model. It is worth mentioning that, in the jump condition of the momentum balance, we identify the square-gradient term of the

free energy as the surface tension (5.19) of our phase-field model. We further relate it to the physical surface tension through a ratio parameter, where a relation (5.25) is provided to determine the value of this parameter.

We also compute three examples, including thermocapillary convection in a two-layer fluid system and thermocapillary migration of a drop. The results for the first two examples are in good agreement with the existing analytical and numerical solutions quantitatively, which validates our phase-field model. Thus, on the whole, we conclude that the phase-field model is very suitable for simulating multiphase flows with thermocapillary effects.

In future work, apart from exploring various applications and extensions of the model, we intend to provide an asymptotic analysis of the solution of the model, and use it as a further validation of our model. For the phase-field model developed here, we will present a thermodynamic consistency preserving numerical method with the corresponding numerical results in a forthcoming work (Guo & Lin 2014).

Acknowledgements

Z.G. was partially supported by the Chinese Scholarship Council (no. 2011646021) for study at the University of Dundee. P.L. was partially supported by the Fundamental Research Funds for Central Universities (nos 06108038 and 06108137).

REFERENCES

- ABELS, H. & FEIREISL, E. 2008 On a diffuse interface model for a two-phase flow of compressible viscous fluids. *Indiana Univ. Math. J.* **57**, 659–698.
- ABELS, H., GARCKE, H. & GRUN, G. 2010 Thermodynamically consistent diffuse interface models for incompressible two-phase flows with different densities. [arXiv:1011.0528](https://arxiv.org/abs/1011.0528).
- ABELS, H., GARCKE, H. & GRÜN, G. 2012 Thermodynamically consistent, frame invariant, diffuse interface models for incompressible two-phase flows with different densities. *Math. Models Meth. Appl. Sci.* **22** (3), 1150013.
- AKI, G. L., DREYER, W., GIESSELMANN, J. & KRAUS, C. 2014 A quasi-incompressible diffuse interface model with phase transition. *Math. Models Meth. Appl. Sci.* **24** (5), 827–861.
- ALAND, S. 2012 Modelling of two-phase flow with surface active particles. PhD thesis, TU Dresden.
- ALAND, S. & VOIGT, A. 2012 Benchmark computations of diffuse interface models for two-dimensional bubble dynamics. *Intl J. Numer. Meth. Fluids* **69**, 747–761.
- ALLAIRE, G., CLERC, S. & KOKH, S. 2002 A five-equation model for the simulation of interface between compressible fluids. *J. Comput. Phys.* **181**, 577–616.
- ANDERECK, C. D., COLOVAS, P. W., DEGEN, M. M. & RENARDY, Y. Y. 1998 Instabilities in two layer Rayleigh–Bénard convection: overview and outlook. *Intl J. Engng Sci.* **36**, 1451.
- ANDERSON, D. M. & MCFADDEN, G. B. 1996 A diffuse-interface description of fluid systems. In *NIST IR 5887*, National Institute of Standards and Technology.
- ANDERSON, D. M., MCFADDEN, G. B. & WHEELER, A. A. 1998 Diffuse-interface methods in fluid mechanics. *Annu. Rev. Fluid Mech.* **30**, 139–165.
- ANDERSON, D. M., MCFADDEN, G. B. & WHEELER, A. A. 2000 A phase-field model of solidification with convection. *Physica D* **135**, 175–194.
- ANDERSON, D. M., MCFADDEN, G. B. & WHEELER, A. A. 2001 A phase-field model with convection: sharp-interface asymptotics. *Physica D* **151**, 305–331.
- ANDREA, D. 2011 Equations for two-phase flows: a primer. [arXiv:1101.5732v1](https://arxiv.org/abs/1101.5732v1) [physics.flu-dyn].
- ANTANOVSKII, L. K. 1995 A phase field model of capillarity. *Phys. Fluids* **7**, 747–753.
- BALDALASSI, V., CENICEROS, H. & BANERJEE, S. 2004 Computation of multiphase systems with phase field models. *J. Comput. Phys.* **190**, 371–397.

- BAO, K., SHI, Y., SUN, S. & WANG, X.-P. 2012 A finite element method for the numerical solution of the coupled Cahn–Hilliard and Navier–Stokes system for moving contact line problems. *J. Comput. Phys.* **231**, 8083–8099.
- BATCHELOR, G. K. 2000 *An Introduction to Fluid Dynamics*. Cambridge University Press.
- BÉNARD, H. 1900 Les tourbillons cellulaires dans une nappe liquide. Première partie: description. *Rev. Gen. Sci. Pure Appl.* **11**, 1261–1271.
- BEREJNOV, V., LAVRENTEVA, O. M. & NIR, A. 2001 Interaction of two deformable viscous drops under external temperature gradient. *J. Colloid Interface Sci.* **242**, 202–213.
- BLESGEN, T. 1999 A generalization of the Navier–Stokes equations to two-phase flows. *J. Phys. D: Appl. Phys.* **32** (10), 1119.
- BLOCK, M. J. 1956 Surface tension as the cause of Benard cells and surface deformation in a liquid film. *Nature* **178**, 650–651.
- BLYTH, M. G. & POZRIKIDIS, C. 2004 Effect of inertia on the Marangoni instability of two-layer channel flow, part II: normal-mode analysis. *J. Engng Maths* **50**, 329–341.
- BORCIA, R. & BESTEHORN, M. 2003 Phase-field for Marangoni convection in liquid–gas systems with a deformable interface. *Phys. Rev. E* **67**, 066307.
- BORCIA, R., MERKT, D. & BESTEHORN, M. 2004 A phase-field description of surface-tension-driven instability. *Intl J. Bifurcation Chaos* **14** (12), 4105–4116.
- BOYER, F. 2002 A theoretical and numerical model for the study of incompressible mixture flows. *Comput. Fluids* **31**, 41–68.
- CAHN, J. W. & ALLEN, S. M. 1978 A microscopic theory for domain wall motion and its experimental verification in Fe–Al alloy domain growth kinetics. *J. Phys. Colloq. C* **38**, 7–51.
- CAHN, J. W. & HILLIARD, J. E. 1958 Free energy of a nonuniform system I: interfacial free energy. *J. Chem. Phys.* **28**, 258–267.
- CHELLA, R. & VINALS, J. 1996 Mixing of a two-phase fluid by cavity flow. *Phys. Rev. E* **53**, 3832–3840.
- DARHUBER, A. A. & TROIAN, S. M. 2005 Principles of microfluidic actuation by modulation of surface stresses. *Annu. Rev. Fluid Mech.* **37**, 425–455.
- DAVIS, S. H. 1987 Thermocapillary instabilities. *Annu. Rev. Fluid Mech.* **19**, 403–435.
- DING, H., SPELT, P. D. M. & SHU, C. 2007 Diffuse interface model for incompressible two-phase flows with large density ratios. *J. Comput. Phys.* **226**, 2078–2095.
- ECK, C., FONTELOS, M., GRUN, G., KLINGBEIL, F. & VANTZOS, O. 2009 On a phase-field model for electrowetting. *Interfaces Free Bound.* **11** (2), 259–290.
- EMMERICH, H. 2008 Advances of and by phase-field modelling in condensed-matter physics. *Adv. Phys.* **57** (1), 1–87.
- EVERETT, D. H. 1972 Definitions, terminology and symbols in colloid and surface chemistry. *Pure Appl. Chem.* **31**, 577.
- GAMBARYAN-ROISMAN, T., ALEXEEV, A. & STEPHAN, P. 2005 Effect of the microscale wall topography on the thermocapillary convection within a heated liquid film. *Exp. Therm. Fluid Sci.* **29**, 765–772.
- GAO, M. & WANG, X.-P. 2012 A gradient stable scheme for a phase field model for the moving contact line problem. *J. Comput. Phys.* **231**, 1372–1386.
- GARCKE, H., HINZE, M. & KAHLE, C. 2014 A stable and linear time discretization for a thermodynamically consistent model for two-phase incompressible flow. [arXiv:1402.6524](https://arxiv.org/abs/1402.6524).
- GIBBS, J. W. 1875 On the equilibrium of heterogeneous substances. *Trans. Connect. Acad.* **3**, 109.
- GIBBS, J. W. 1928 *The Collected Works of J. W. Gibbs*. Longmans and Green.
- GIESSELMANN, J. & PRYER, T. 2013 Energy consistent discontinuous Galerkin methods for a quasi-incompressible diffuse two phase flow model. <http://archiv.org/abs/1307.8248>.
- GINZBURG, V. L. & LANDAU, L. D. 1950 Theory of superconductivity. *Zh. Eksp. Teor. Fiz.* **20**, 1064–1082.
- GROOT, S. R., DE & MAZUR, P. 1985 *Non-Equilibrium Thermodynamics*. Dover Books on Physics.
- GRUN, G. 2013 On convergent schemes for diffuse interface models for two-phase flow of incompressible fluids with general mass densities. *SIAM J. Numer. Anal.* **51** (6), 3036–3061.

- GRUN, G. & KLINGBEIL, F. 2014 Two-phase flow with mass density contrast: stable schemes for a thermodynamic consistent and frame-indifferent diffuse interface model. *J. Comput. Phys.* **257**, 708–725.
- GUO, Z. & LIN, P. 2014 A thermodynamic consistency preserving numerical method for a phase-field model with thermocapillary effects (in preparation).
- GUO, Z., LIN, P. & LOWENGRUB, J. 2014 A numerical method for the quasi-incompressible Cahn–Hilliard–Navier–Stokes equations for variable density flows with a discrete energy law. *J. Comput. Phys.* **276**, 486–507.
- GUO, Z., LIN, P. & WANG, Y. 2014*b* Continuous finite element schemes for a phase field model in two-layer fluid Bénard–Marangoni convection computations. *Comput. Phys. Commun.* **185**, 63–78.
- GURTIN, M. E., POLIGONE, D. & VINALE, J. 1996 Two-phase fluids and immiscible fluids described by an order parameter. *Math. Models Meth. Appl. Sci.* **6**, 815–831.
- HAIJ-HARIRI, H., SHI, Q. & BORHAN, A. 1997 Thermocapillary motion of deformable drops at finite Reynolds and Marangoni numbers. *Phys. Fluids* **9**, 845–855.
- HE, Q., GLOWINSKI, R. & PING, X. 2011 A least-squares/finite element method for the numerical solution of the Navier–Stokes–Cahn–Hilliard system modeling the motion of the contact line. *J. Comput. Phys.* **230**, 4991–5009.
- HERRMANN, M., LOPEZ, J. M., BRADY, P. & RAESSI, M. 2008 Thermocapillary motion of deformable drops and bubbles. In *Proceedings of the 2008 Summer Program* (ed. P. Moin, N. N. Mansour & D. You), pp. 155–170. Center for Turbulence Research, Stanford University.
- HOHENBERG, P. C. & HALPERIN, B. I. 1977 Theory of dynamic critical phenomena. *Rev. Mod. Phys.* **49**, 435–479.
- HOU, T. Y., LOWENGRUB, J. S. & SHELLEY, M. J. 2001 Boundary integral methods for multicomponent fluids and multiphase materials. *J. Comput. Phys.* **169**, 302–362.
- HUA, J., LIN, P., LIU, C. & WANG, Q. 2011 Energy law preserving C^0 finite element schemes for phase field models in two-phase flow computations. *J. Comput. Phys.* **230**, 7115–7131.
- HUA, J. S., STENE, J. F. & LIN, P. 2008 Numerical simulation of 3d bubbles rising in viscous liquids using a front tracking method. *J. Comput. Phys.* **227** (6), 3358–3382.
- JACQMIN, D. 1999 Calculation of two-phase Navier–Stokes flows using phase-field modeling. *J. Comput. Phys.* **155**, 96–127.
- JACQMIN, D. 2000 Contact-line dynamics of a diffuse fluid interface. *J. Fluid Mech.* **402**, 57–88.
- JASNOW, D. & VINALS, J. 1996 Coarse-grained description of thermo-capillary flow. *Phys. Fluids* **8**, 660–669.
- JIANG, Y. & LIN, P. 2014 Numerical simulation for moving contact line with continuous finite element schemes (in press).
- KIM, J. 2005 A continuous surface tension force formulation for diffuse-interface models. *J. Comput. Phys.* **204**, 784–804.
- KIM, J. 2012 Phase-field models for multi-component fluid flows. *Commun. Comput. Phys.* **12** (3), 613–661.
- KIM, J., KANG, K. & LOWENGRUB, J. 2004 Conservative multigrid methods for Cahn–Hilliard fluids. *J. Comput. Phys.* **193**, 511–543.
- KIM, J. & LOWENGRUB, J. 2005 Phase field modelling and simulation of three-phase flows. *Interface Free Bound.* **7**, 435–466.
- LEE, H. G., LOWENGRUB, J. & GOODMAN, J. 2002*a* Modeling pinchoff and reconnection in a Hele–Shaw cell. I. The models and their calibration. *Phys. Fluids* **14** (2), 492–513.
- LEE, H. G., LOWENGRUB, J. & GOODMAN, J. 2002*b* Modeling pinchoff and reconnection in a Hele–Shaw cell. II. Analysis and simulation in the nonlinear regime. *Phys. Fluids* **14** (2), 514–545.
- LEVICH, V. G. 1962 *Physicochemical Hydrodynamics*. Prentice-Hall.
- LIN, P. & LIU, C. 2006 Simulation of singularity dynamics in liquid crystal flows: a C^0 finite element approach. *J. Comput. Phys.* **215** (1), 348–362.

- LIN, P., LIU, C. & ZHANG, H. 2007 An energy law preserving C^0 finite element scheme for simulating the kinematic effects in liquid crystal flow dynamics. *J. Comput. Phys.* **227** (2), 1411–1427.
- LIU, C. & SHEN, J. 2002 A phase field model for the mixture of two incompressible fluids and its approximation by a Fourier-spectral method. *Physica D* **179**, 211–228.
- LIU, H., VALOCCHI, A. J., ZHANG, Y. & KANG, Q. 2014 Lattice Boltzmann phase-field modeling of thermocapillary flows in a confined microchannel. *J. Comput. Phys.* **256**, 334–356.
- LOWENGRUB, J. & TRUSKINOVSKY, L. 1998 Quasi-incompressible Cahn–Hilliard fluids and topological transitions. *Proc. R. Soc. Lond. A* **454**, 2617–2654.
- MA, C. & BOTHE, D. 2013 Numerical modeling of thermocapillary two-phase flows with evaporation using a two-scalar approach for heat transfer. *J. Comput. Phys.* **233**, 552–573.
- MASE, G. E. & MASE, G. T. 1999 *Continuum Mechanics for Engineers*, 2nd edn. CRC Press.
- MITTAL, R. & IACCARINO, G. 2005 Immersed boundary methods. *Annu. Rev. Fluid Mech.* **37**, 239–361.
- MORAN, M. J., SHAPIRO, H. N., BOETTNER, D. D. & BAILEY, M. 2010 *Fundamentals of Engineering Thermodynamics*, 7th edn. Wiley.
- NAS, S., MURADOGU, M. & TRYGGVASON, G. 2006 Pattern formation of drops in thermocapillary migration. *Intl J. Heat Mass Transfer* **49**, 2265–2276.
- NAS, S. & TRYGGVASON, G. 2003 Thermocapillary interaction of two bubbles or drops. *Intl J. Multiphase Flow* **29**, 1117–1135.
- OSHER, S. J. & FEDKIW, R. P. 2001 Level set methods: An overview and some recent results. *J. Comput. Phys.* **169**, 463–502.
- PEARSON, J. R. A. 1958 On convection cells induced by surface tension. *J. Fluid Mech.* **4**, 489–500.
- PENDSE, B. & ESMAEELI, A. 2010 An analytical solution for thermocapillary-driven convection of superimposed fluids at zero Reynolds and Marangoni numbers. *Intl J. Therm. Sci.* **49**, 1147–1155.
- POZRIKIDIS, C. 2004 Effect of inertia on the Marangoni instability of two-layer channel flow, Part I: numerical simulations. *J. Engng Maths* **50**, 311–327.
- QIAN, T., WANG, X. & SHENG, P. 2006 Molecular hydrodynamics of the moving contact line in two-phase immiscible flows. *Commun. Comput. Phys.* **1** (1), 1–52.
- ROTHER, M. A., ZINCHENKO, A. Z. & DAVIS, R. H. 2002 A three-dimensional boundary-integral algorithm for thermocapillary motion of deformable drops. *J. Colloid Interface Sci.* **245**, 356–364.
- ROWLINSON, J. S. & WIDOM, B. 1982 *Molecular Theory of Capillarity*. Dover.
- SCARDOVELLI, R. & ZALESKI, S. 1999 Direct numerical simulation of free surface and interfacial flows. *Annu. Rev. Fluid Mech.* **31**, 567–603.
- SCHATZ, M. F. & NEITZEL, G. P. 2001 Experiments on thermocapillary instabilities. *Annu. Rev. Fluid Mech.* **33**, 93–127.
- SCRIVEN, L. E. & STERNLING, C. V. 1964 On cellular convection driven by surface tension gradient: effects of mean surface tension and viscosity. *J. Fluid Mech.* **19**, 321–340.
- SEKERKA, R. F. 1993 Notes on entropy production in multicomponent fluids (unpublished).
- SETHIAN, J. A. & SMERKA, P. 2003 Level set methods for fluid interfaces. *Annu. Rev. Fluid Mech.* **35**, 341–372.
- SHEN, J. & YANG, X. 2009 An efficient moving mesh spectral method for the phase-field model of two-phase flows. *J. Comput. Phys.* **228**, 2978–2992.
- SHEN, J. & YANG, X. 2010 A phase-field model and its numerical approximation for two-phase incompressible flows with different densities and viscosities. *SIAM J. Sci. Comput.* **33**, 1159–1179.
- VAN DER SMAN, R. G. M. & VAN DER GRAAF, S. 2006 Diffuse interface model of surfactant adsorption onto flat and droplet interfaces. *Rheol. Acta* **46**, 3–11.
- STERNLING, C. V. & SCRIVEN, L. E. 1959 Interfacial turbulence: hydrodynamic instability and the Marangoni effect. *AIChE J.* **5**, 514–523.
- SUBRAMANIAN, R. S. & BALASUBRAMANIAM, R. 2001 *The Motion of Bubbles and Drops in Reduced Gravity*. Cambridge University Press.

- SUN, P., LIU, C. & XU, J. 2009 Phase field model of thermo-induced Marangoni effects in the mixtures and its numerical simulations with mixed finite element method. *Commun. Comput. Phys.* **6**, 1095–1117.
- TAVENER, S. J. & CLIFFE, K. A. 2002 Two-fluid Marangoni–Bénard convection with a deformable interface. *J. Comput. Phys.* **182**, 277–300.
- TEIGEN, K. E., SONG, P., LOWENGRUB, J. & VOIGT, A. 2011 A diffuse-interface method for two-phase flows with soluble surfactants. *J. Comput. Phys.* **230**, 375–393.
- TRYGGVASON, G., BUNNER, B., ESMAEELI, A., JURIC, D., AL-RAWAHI, N., TAUBER, W., HAN, J., NAS, S. & JAN, Y. J. 2001 Front tracking method for the computation of multiphase flow. *J. Comput. Phys.* **169**, 708–759.
- TRYGGVASON, G., SCARDOVELLI, R. & ZALESKI, S. 2011 *Direct Numerical Simulations of Gas–Liquid Multiphase Flows*. Cambridge University Press.
- VERSCHUEREN, M., VAN DE VOSSE, F. N. & MEIJER, H. E. H. 2001 Diffuse-interface modelling of thermo-capillary flow instabilities in a Hele-Shaw cell. *J. Fluid Mech.* **434**, 153–166.
- VAN DER WAALS, J. D. 1979 The thermodynamic theory of capillary flow under the hypothesis of a continuous variation of density. *J. Stat. Phys.* **20**, 197 (English translation).
- WANG, S. L., SEKERKA, R. F., WHEELER, A. A., MURRAY, B. T., CORIELL, S. R., BRAUN, R. J. & MCFADDEN, G. B. 1993 Thermodynamically-consistent phase-field models for solidification. *Physica D* **69**, 189–200.
- WANG, X.-P. & WANG, Y.-G. 2007 The sharp interface limit of a phase field model for moving contact line problem. *Meth. Appl. Anal.* **14** (3), 285–292.
- WEATHERBURN, C. E. 1939 *Differential Geometry of Three Dimensions*. Cambridge University Press.
- YIN, Z., GAO, P., HU, W. & CHANG, L. 2008 Thermocapillary migration of nondeformable drops. *Phys. Fluids* **20**, 082101.
- YOUNG, N. O., GOLDSTEIN, J. S. & BLOCK, M. J. 1959 The motion of bubbles in a vertical temperature gradient. *J. Fluid Mech.* **6**, 350–356.
- YUE, P. & FENG, J. J. 2012 Phase-field simulations of dynamic wetting of viscoelastic fluids. *J. Non-Newtonian Fluid Mech.* **189**, 8–13.
- YUE, P., FENG, J. J., LIU, C. & SHEN, J. 2004 A diffuse interface method for simulating two phase flows of complex fluids. *J. Fluid Mech.* **515**, 293–317.
- YUE, P., ZHOU, C. F., FENG, J. J., OLLIVIER-GOOCH, C. F. & HU, H. H. 2006 Phase-field simulations of interfacial dynamics in viscoelastic fluids using finite elements with adaptive meshing. *J. Comput. Phys.* **219** (1), 47–67.
- ZHAO, J., LI, Z., LI, H. & LI, J. 2010 Thermocapillary migration of deformable bubbles at moderate to large Marangoni number in microgravity. *Microgravity Sci. Technol.* **22**, 295–303.
- ZHOU, H. & DAVIS, R. H. 1996 Axisymmetric thermocapillary migration of two deformable viscous drops. *J. Colloid Interface Sci.* **181**, 60–72.